

Kernel-based estimators for functional causal effects

Yordan P. Raykov¹, Hengrui Luo², Justin D. Strait³, and Wasiur R. KhudaBuksh⁴

¹School of Mathematical Sciences, Horizon Digital Economy Institute, University of Nottingham, Nottingham, UK

²Department of Statistics, Rice University, USA; Lawrence Berkeley National Laboratory, USA

³Statistical Sciences Group, Los Alamos National Laboratory, USA

⁴School of Mathematical Sciences, University of Nottingham, Nottingham, UK

Abstract

We propose causal effect estimators based on empirical Fréchet means and operator-valued kernels, tailored to functional data spaces. These methods address the challenges of high-dimensionality, sequential ordering, and model complexity while preserving robustness to treatment misspecification. Using structural assumptions, we obtain compact representations of potential outcomes, enabling scalable estimation of causal effects over time and across covariates. We provide both theoretical regarding the consistency of functional causal effects, as well as empirical comparison of a range of proposed causal effect estimators.

Applications to binary treatment settings with functional outcomes illustrate the framework's utility in biomedical monitoring, where outcomes exhibit complex temporal dynamics. Our estimators accommodate scenarios with registered covariates and outcomes, aligning them to the Fréchet means, as well as cases requiring higher-order representations to capture intricate covariate-outcome interactions. These advancements extend causal inference to dynamic and non-linear domains, offering new tools for understanding complex treatment effects in functional data settings.

1 Introduction

1.1 Background

Causal inference frameworks are often motivated by the desire to estimate causal effects from associational terms computed from observed data. Much of the conventional literature on causal analysis is based on longitudinal observational studies, such as clinical trials and prospective studies, where different configurations of exposure, covariates, and outcome variables are observed at single (Rosenbaum and Rubin, 1983) or multiple time points (Robins et al., 2000). Experimenters make choices about the exposure mapping or intervention in their causal model, adopting different adjustment procedures depending on whether treatment regimes are statically assigned (i.e., at baseline) (Robins et al., 2000), dynamically optimized (Murphy, 2003), time-dependent, or constant over time (Pearl and Robins, 1995). Modern applications often involve measurements at various time scales, providing opportunities to study causal effects between variables that follow different temporal dynamics, which are essentially functional data.

Specifically, we study the problem of *estimating the causal effect when covariates and/or outcomes are functional data*. We demonstrate that causal models, equipped with suitable distance

metrics for functional data, facilitate more efficient estimators with well-motivated properties, capable of capturing causal effects over different time scales. The primary focus of this work is distinct from designing causal models for time-dependent exposure and treatment strategies detailed in [Robins et al. \(2000\)](#). Instead, our contribution addresses estimating causal effects on complex object spaces ([Lin et al., 2023](#); [Kennedy et al., 2023](#); [Testa et al., 2025](#); [Kurisu et al., 2024](#)), which becomes a prerequisite for the larger challenge of studying time-changing exposures ([Robins et al., 2000](#); [Murphy, 2003](#)). Our immediate goal is to estimate both scalar and path-valued effects of an exposure on a path-valued functional outcome, potentially extending to multiple time scales ([Daniel et al., 2013](#)).

Causal inference methods for more complex outcomes have gained traction only recently. For example, [Lin et al. \(2023\)](#) considers distributional differences in generalized Wasserstein space for scalar potential outcomes, while [Kurisu et al. \(2024\)](#) generalizes treatment effect estimation to outcomes in geodesic metric spaces. In our work, the outcomes themselves are more complex, and we introduce a joint aligning-kernelization procedure to estimate causal effects over the mean potential outcomes under both binary and continuous treatments. Previous investigations of binary treatment effects for path-valued outcomes include [Belloni et al. \(2017\)](#), who develops approximate local treatment effect estimators for non-Euclidean outcomes (forgoing finite-sample inference), and [Ecker et al. \(2024\)](#), who uses function-on-scalar regression under a linear parametric assumption. More recently, [Testa et al. \(2025\)](#) and [Kurisu et al. \(2024\)](#) propose doubly robust frameworks for complex outcomes. [Testa et al. \(2025\)](#) derives point-wise doubly robust estimators for path-valued outcomes in L_2 , and [Kurisu et al. \(2024\)](#) leverages known geodesic metric spaces to estimate scalar-valued treatment effects. Our kernel-based approach differs in that it does not center on doubly robust properties. Instead, for outcomes in known geodesic spaces, our scalar φ^{dATE} estimator can be seen as a special case of [Kurisu et al. \(2024\)](#)’s *geodesic average treatment effect*, and for outcomes in L_2 , our point-wise effect $\Delta(t)$ aligns with [Testa et al. \(2025\)](#)’s estimator. Moreover, we consider practical settings where outcomes may not be truly infinite-dimensional or where the associated geodesic is unknown, in which case we employ nonparametric kernel ridge regression and *square root slope transformations*.

By adopting a nonparametric paradigm for causal effect estimation, our framework covers a more general setting than [Belloni et al. \(2017\)](#) and [Ecker et al. \(2024\)](#), and it explicitly addresses a broader range of causal effects motivated by functional outcomes and/or covariates. In contrast to [Testa et al. \(2025\)](#), which focuses on doubly robust estimators, we emphasize kernel-based causal estimation, thus providing an alternative route for practitioners wishing to avoid strong structural assumptions. Our estimators can also be viewed as special cases of conditional average treatment effects, where conditioning occurs on discrete points along the path grid. Crucially, we argue that leveraging a richer representation of outcome structure can improve precision and mitigate potential collider stratification bias ([Daniel et al., 2013](#)).

The proposed path-valued functional potential outcomes remain sensitive to the exposure probability specification (i.e., the propensity score) and expected outcome models ([Sävje, 2024](#)). Building on the kernel-based estimators from [Singh et al. \(2020\)](#), we develop a nonparametric framework that implicitly incorporates the propensity score, eliminating the need for its direct inversion. We extend these estimators to multivariate and infinite-dimensional outcomes by defining purpose-designed operator-valued kernels ([Kadri et al., 2016](#)), and we further demonstrate how the *Fisher–Rao* metric can embed outcome and covariate registration directly into functional causal inference. This preserves both theoretical guarantees of consistency for the expected potential outcome estimators and practical advantages, as illustrated empirically.

Finally, we showcase the utility of our framework for estimating causal effects from digital outcomes in Parkinson’s Disease (PD). Using data from the Parkinson@Home validation study—a

passive monitoring study involving 50 participants¹—we estimate the effects of levodopa therapy and disease status (PD vs. age-matched non-PD controls). Our higher-dimensional estimators uncover significant disease-related impacts on recorded digital outcomes that often remain undetectable using standard aggregated measures.

1.2 Illustration

To illustrate the concepts, consider an example in digital monitoring of Parkinson’s disease (PD) (Evers et al., 2020; Bloem et al., 2019), where a treatment X captures daily levodopa-equivalent dosage decisions. Typically, these decisions are set at the start of the day (e.g., total dosage or allocation strategy), rather than intervening anew at every intake event. Meanwhile, the outcome $Y(t)$ measures PD symptoms (e.g., tremor or bradykinesia) at different times t throughout the day.

We explore two approaches to modeling X :

1. **Marginal Exposure Models.** Here, $X \in \{0, 1\}$ simply indicates whether any medication is used during the day (or not). This collapses potentially complex dosing schedules into a single binary indicator, yielding a uniform “exposure vs. non-exposure” comparison across the entire day.
2. **Continuous Treatment Variable.** In this approach, $X \in \mathbb{R}^+$ is a single, scalar quantity (e.g., total daily dosage) that may also encode timing or frequency of intake (through weights or other aggregation). Although assigned once at baseline, this continuous measure allows for more nuanced estimation of how varying dosage levels influence the outcome $Y(t)$ over the course of the day.

By avoiding frequent redefinition of X at each intake event, these two formulations capture realistic clinical scenarios where daily dosage plans are decided once and then implemented. This also facilitates studying how a single day-level treatment choice affects the dynamic evolution of symptoms $Y(t)$. Each observed (X, Y) can be augmented with covariates $V(t)$, which may vary at different time scales (e.g., age, activity levels, diurnal patterns). Under mild smoothness assumptions, we propose estimators that measure the effect of these treatment variables on the functional outcomes $\{Y(t)\}_{t \in [0,1]}$. The rest of the paper is structured as follows: in Section 2, we provide a brief overview of the causal inference methods applicable to our setup. We discuss binary treatment with functional outcomes in Section 3, while in Section 4 we consider kernel-based causal effect estimators which also facilitate nonparametric inference in the case of continuous treatments. We present empirical comparison of different causal effect estimators in Section 5 and also evaluate the feasibility of the digital monitoring of PD with the novel causal estimators. Some limitations of the proposed approach and future directions are summarized in Section 6.

2 Casual Inference Preliminaries

To motivate our setting of function-valued treatment and function-valued outcomes, we first define causal effects in the scalar case using potential outcome notation. Treatments are denoted as $X = x$, where x can be either 0 or 1 for binary treatment exposure, or $x \in \mathbb{R}^+$ for dose-response exposure. Let $\mathbf{V} \in \mathbb{R}^d$ denote the observed baseline covariates that influence both the treatment X and the outcome Y . For each treatment level x , the potential outcome $Y^{(x)}$ represents the outcome that

¹The 2-week follow-up passive monitoring data from the Parkinson@Home validation study is also made available with this study.

would have been observed had the subject received treatment x . The potential outcome $Y^{(x)}$ is counterfactual and distinct from the observed conditional expectation $\mathbb{E}[Y | X = x]$, which depends on observed treatment assignments. Inferring $\mathbb{E}[Y^{(x)}]$ from observational data requires assumptions on how the baseline covariates \mathbf{V} influence both treatment and outcome (Hernán and Robins, 2010; Rosenbaum and Rubin, 1983; Robins et al., 1994). Specifically, \mathbf{V} must satisfy either the *back-door criterion* or the *front-door criterion* with respect to (X, Y) (see Appendix A for details).

If \mathbf{V} satisfies the back-door criterion with respect to (X, Y) , the potential outcome expectation can be identified via covariate adjustment:

$$\mathbb{E}[Y^{(x)}] = \int_{\mathcal{V}} \mathbb{E}[Y | X = x, \mathbf{V} = \mathbf{v}] dP_{\mathbf{V}}(\mathbf{v}). \quad (1)$$

If instead a set of covariates \mathbf{V} satisfies the front-door criterion, identification follows from a different factorization (Pearl, 1995):

$$\mathbb{E}[Y^{(x)}] = \int_{\mathcal{X}} \left(\int_{\mathcal{V}} \mathbb{E}[Y | X = x', \mathbf{V} = \mathbf{v}] dP_{\mathbf{V}|X}(\mathbf{v} | x) \right) P_X(dx'), \quad (2)$$

where the treatment probability is marginalized due to its causal effect on \mathbf{V} . For binary treatments $x \in \{0, 1\}$, this simplifies to a weighted sum of the expected outcomes in the treated and non-treated groups, adjusted for intermediate confounders.

Causal effects are derived from counterfactual potential outcomes. Assume n independent samples drawn from a superpopulation of (X, \mathbf{V}, Y) , denoted as (X_i, \mathbf{V}_i, Y_i) for $i = 1, \dots, n$. The covariates matrix is:

$$\mathbf{V} = \begin{pmatrix} \mathbf{V}_1 \\ \vdots \\ \mathbf{V}_n \end{pmatrix} \in \mathbb{R}^{n \times d},$$

where each row represents an individual and each column a covariate. For binary exposure $X \in \{0, 1\}$, we measure the *average treatment effect* as a contrast measure between the potential outcomes:

$$\begin{aligned} \varphi^{ATE} &= \mathbb{E}[Y^{(1)}] - \mathbb{E}[Y^{(0)}] \\ &= \int \varphi^{ATE}(\mathbf{v}) dP_{\mathbf{V}}(\mathbf{v}), \quad (\text{Binary treatment effect}) \end{aligned} \quad (3)$$

where the *heterogeneous treatment effect* for covariates $\mathbf{V} = \mathbf{v}$ is:

$$\varphi^{ATE}(\mathbf{v}) = \mathbb{E}[Y^{(1)} | \mathbf{V} = \mathbf{v}] - \mathbb{E}[Y^{(0)} | \mathbf{V} = \mathbf{v}]. \quad (4)$$

In the case of continuous exposure $X \in \mathbb{R}^+$ and $Y^{(x)} \in \mathbb{R}$, simple contrast measures like the above ATE score are not appropriate since the difference between two continuous levels x_1 and x_2 may be influenced by intermediate levels in a cumulative manner. Instead, the dose-response function for each level x of X is the key effect of interest:

$$\varphi^{DS}(x) = \mathbb{E}[Y^{(x)}] \quad (\text{Dose-response effect}) \quad (5)$$

where the formula for $\varphi^{DS}(x)$ in terms of observational terms takes the form of (1) or (2) depending on whether back-door or front-door criterion for \mathbf{V} on (X, Y) are being met.

Estimating causal effects from observational data involves translating the population-level formulas (e.g., (3)) into empirical estimators that use observed samples. The validity of these estimators depends on whether back-door or front-door conditions hold and on certain regularity assumptions. A common set of assumptions is the so-called *unconfoundedness* (or *ignorability*) condition, which is typically aligned with the back-door criterion:

Assumption 1. (Ignorability) $X \perp Y^{(x)} \mid \mathbf{V}$, for any $X = x$.

Assumption 2. (Positivity) The propensity score $\pi(\mathbf{V}) = p(X = 1 \mid \mathbf{V})$ is bounded away from 0 and 1, almost everywhere. That is, $\exists \epsilon > 0$ such that $\epsilon < \pi(\mathbf{V}) < 1 - \epsilon$.

In the back-door scenario, Assumption 1 ensures that once we condition on \mathbf{V} , the distribution of the potential outcomes is no longer confounded by unobserved variables. Assumption 2 ensures we have sufficient variability in treatment assignment across values of \mathbf{V} to estimate causal effects. For front-door identification, a different set of conditions apply, involving sequential ignorability assumptions that allow factorizing the observational distribution as in (2). The estimators discussed next are standard approaches primarily under the back-door setup, though similar logic can be extended or adapted for front-door adjustments with more complex estimators. Under the back-door criterion, the potential outcome expectations simplify to:

$$\mathbb{E}[Y^{(1)}] = \mathbb{E} \left[\frac{XY}{\pi(\mathbf{V})} \right], \quad \mathbb{E}[Y^{(0)}] = \mathbb{E} \left[\frac{(1-X)Y}{1-\pi(\mathbf{V})} \right].$$

These expressions allow constructing sample-based estimators. Given n independent and identically distributed (i.i.d.) samples (X_i, \mathbf{V}_i, Y_i) , the *Inverse Probability Weighting* (IPW) estimator of the ATE is:

$$\hat{\varphi}^{IPW} = \frac{1}{n} \sum_{i=1}^n \left(\frac{X_i Y_i}{\hat{\pi}(\mathbf{V}_i)} - \frac{(1-X_i) Y_i}{1-\hat{\pi}(\mathbf{V}_i)} \right). \quad (6)$$

While IPW is consistent if the propensity score model is correct, it can be inefficient and sensitive to model misspecification. A more robust approach is the *Doubly Robust* (DR) estimator, which augments IPW with outcome models:

$$\hat{\varphi}^{DR-IPW} = \frac{1}{n} \sum_{i=1}^n \left(\frac{X_i(Y_i - \hat{m}_1(\mathbf{V}_i))}{\hat{\pi}(\mathbf{V}_i)} + \hat{m}_1(\mathbf{V}_i) - \frac{(1-X_i)(Y_i - \hat{m}_0(\mathbf{V}_i))}{1-\hat{\pi}(\mathbf{V}_i)} + \hat{m}_0(\mathbf{V}_i) \right), \quad (7)$$

where $\hat{m}_1(\mathbf{V}_i) = \mathbb{E}[Y \mid X = 1, \mathbf{V} = \mathbf{V}_i]$ and $\hat{m}_0(\mathbf{V}_i) = \mathbb{E}[Y \mid X = 0, \mathbf{V} = \mathbf{V}_i]$ are estimated outcome regression models. The DR-IPW estimator is consistent if at least one of the models (the propensity score or the outcome model) is correct, providing a form of robustness not available from IPW alone.

The estimators above illustrate how population-level causal effects, derived under certain identification conditions (notably the back-door criterion here), can be approximated by sample-based empirical estimators. Similar estimation strategies can be adapted if the front-door conditions are met, but the factorization in (2) typically leads to different weighting or regression-based methods. Moreover, for continuous treatments, one can estimate the entire dose-response function $\varphi^{DS}(x)$ by generalizing these strategies, for example, employing kernel or regression-based estimators of $\mathbb{E}[Y \mid X = x, \mathbf{V}]$ and integrating out \mathbf{V} under the appropriate assumptions.

3 Binary Treatment with Functional Outcomes

We focus on *binary treatment with functional outcomes*: a scenario where outcomes are functional outcome exhibiting sequential orderings, and each observed \mathbf{Y}_i is drawn from a covariate-specific path-valued random variable (i.e. the potential outcome). By observing at finite time points, these outcomes \mathbf{Y}_i can also be formatted as T -vector consisting of discretized points from an underlying function of $u \in [0, 1]$. Our analysis distinguishes between these two cases where outcomes are infinite-dimensional with $\mathbf{Y}_i \in L^2([0, 1])$, and those where outcomes are finite-dimensional, with $\mathbf{Y}_i \in \mathbb{R}^T$.

Let $(\Omega, \mathcal{A}, \mathbb{P})$ be a probability space, and let $\mathbf{Y} : (\Omega, \mathcal{A}) \rightarrow (\mathcal{F}, \mathcal{B})$ be a measurable map taking values in a metric space (\mathcal{F}, ϕ) , where \mathcal{B} is the Borel σ -algebra on \mathcal{F} . For each treatment level $x \in \{0, 1\}$, let $\mathbf{Y}^{(x)} : (\Omega, \mathcal{A}) \rightarrow (\mathcal{F}, \mathcal{B})$ denote the corresponding potential outcome. Its *distribution* (or pushforward measure) is denoted by η_x , where for any $A \in \mathcal{B}$, $\eta_x(A) = \mathbb{P}(\mathbf{Y}^{(x)} \in A)$. By choosing different metric spaces (\mathcal{F}, ϕ) such as $(\mathbb{R}^T, \|\cdot\|_2)$ and $(L_2([0, 1]), \|\cdot\|_2)$ our setting covers both infinite and finite-dimensional cases above. By the law of total probability, the measure η_x can be expressed by integrating out the covariates \mathbf{V} , with the identification of the distribution $P_{\mathbf{V}}$ depending on whether the *back-door* or *front-door* criteria are satisfied, and how the joint observational distribution of a superpopulation $(X, \mathbf{V}, \mathbf{Y})$ is used.

Casual estimators are based on this superpopulation $(X, \mathbf{V}, \mathbf{Y})$, where covariates and treatment are assigned at baseline. The baseline assignment is critical, as it ensures that covariates and treatments are predetermined and unaffected by the observed high-dimensional outcomes, allowing the formulation of analogous expressions for potential outcomes and corresponding causal effects. More precisely, under the *back-door* criterion for \mathbf{V} for the covariates, $\mathbf{Y}^{(x)} \perp X \mid \mathbf{V}$, so we write:

$$\begin{aligned} \eta_x(A) &= \int P(\mathbf{Y}^{(x)} \in A \mid \mathbf{V} = \mathbf{v}) dP_{\mathbf{V}}(\mathbf{v}) \\ &= \int P(\mathbf{Y} \in A \mid X = x, \mathbf{V} = \mathbf{v}) dP_{\mathbf{V}}(\mathbf{v}). \end{aligned}$$

Under the *front-door* criterion for \mathbf{V} , the measure can be viewed as:

$$\eta_x(A) = \int P(\mathbf{Y}^{(x)} \in A \mid \mathbf{V}^{(x)} = \mathbf{v}) \underbrace{P_{\mathbf{V}^{(x)}}(d\mathbf{v})}_{\text{distribution of } \mathbf{V} \text{ under } \text{do}(X = x)}.$$

where front-door factorization is used to identify $P_{\mathbf{V}^{(x)}}$ and $P(\mathbf{Y}^{(x)} \in A \mid \mathbf{V}^{(x)} = \mathbf{v})$ from the observational distribution (X, \mathbf{V}, Y) with $P_{\mathbf{V}^{(x)}} = \int_{\mathcal{V}} P(\mathbf{V} = \mathbf{v} \mid X = x') P_X(dx')$.

Suppose we equip the space \mathcal{F} with an appropriate distance function ϕ to form the metric space (\mathcal{F}, ϕ) . Then, we can use *Fréchet means* of the probability measures η_x for $x \in \{0, 1\}$ to formulate a generalization of the expected potential outcomes to the metric space (\mathcal{F}, ϕ) and define corresponding causal effect estimators. Define the *Fréchet 2-mean*² of the probability measure η_x :

$$\begin{aligned} F(\mathbf{Y}^{(x)}) &= \arg \min_{f \in \mathcal{F}} \int_{\mathcal{F}} \phi^2(f, g) d\eta_x(g) \\ &= \arg \min_{f \in \mathcal{F}} \int \left[\int_{\mathcal{F}} \phi^2(f, g) d\eta_x(g \mid \mathbf{V} = \mathbf{v}) \right] dP_{\mathbf{V}}(\mathbf{v}), \end{aligned} \tag{8}$$

Our main results focus on cases when unique Fréchet means exist for both treated and non-treated population, where the uniqueness holds with standard regularity conditions on (\mathcal{F}, ϕ) (Evans and Jaffe, 2024). Later, we formulate casual estimators for the treatment effect between random elements $\mathbf{Y}^{(0)}$ and $\mathbf{Y}^{(1)}$ taking values in a metric space (\mathcal{F}, ϕ) , therefore generalizing the classical estimators to take functional values. Specifically, when there are finitely many samples $\mathbf{Y}_i^{(x)} \in \mathcal{F}, i = 1, \dots, n$ in the support of η_x we can have

$$F(\hat{\mathbf{Y}}_i^{(x)}, i = 1, \dots, n) = \arg \min_{f \in \mathcal{F}} \sum_{i=1}^n \phi^2(f, \mathbf{Y}_i^{(x)}). \tag{9}$$

²We will refer to the Fréchet 2-mean simply as the Fréchet mean for brevity.

When the Fréchet means are unique, they belong to a special class of M -estimators (Huber and Ronchetti, 2011) defined by so-called ρ -loss (i.e., here substituting $\rho = \phi^2$), allowing us to leverage well-developed theory to establish their consistency, robustness and rates of convergence. More general cases where the solution from (8) forms *Fréchet mean sets* inherit only weaker forms of consistency (Schötz, 2022; Evans and Jaffe, 2024).

Assumption 3. (Uniqueness) We assume that (8) and (9) are unique up to probability 1 with respect to probability measure \mathbb{P} .

Definition 1. Let $\mathbf{Y}^{(0)}$ and $\mathbf{Y}^{(1)}$ be random elements taking values in a metric space (\mathcal{F}, ϕ) , with corresponding probability distributions η_0 and η_1 . Assume that each has *the unique* Fréchet mean in \mathcal{F} , defined by (8) for $x \in \{0, 1\}$. We define the scalar *dynamic average treatment effect* by

$$\varphi^{dATE} = \phi(F(\mathbf{Y}^{(1)}), F(\mathbf{Y}^{(0)})). \quad (10)$$

This is the distance of the Fréchet means in (\mathcal{F}, ϕ) .

Remark 2. For sets of generalized Fréchet means (Aveni and Mukherjee, 2024), the minimizer defined in (8) is non-unique, we can define the dynamic treatment effect using the Hausdorff distance $d_H(\cdot, \cdot)$ between the Fréchet mean sets:

$$\varphi^{dATE} = d_H(F_M(\mathbf{Y}^{(1)}), F_M(\mathbf{Y}^{(0)})), \quad (11)$$

where $F_M(\mathbf{Y}^{(x)})$ denotes the Fréchet mean set for treatment x to extend our approaches. Unfortunately, such set-valued estimators arising as Fréchet means are less amenable to classical asymptotic analysis because the Hausdorff distance in set space is not differentiable, which impedes the application of central limit theorems without imposing additional structure.

The consistency of φ^{dATE} and the asymptotic normality of the estimation residual which would allow us to leverage existing theory when estimating the significance of an estimated effect require a few additional assumptions which we specify more formally below.

3.1 Discretization of Functional Outcome

In practical applications, it is common to assume access to finitely many points $\mathbf{Y}_i^{(x)} \in \mathbb{R}^T$ sampled from \mathcal{F} on a shared fixed grid $\{u_t\}_{t=1}^T$ with T points on $[0, 1]$. Under this discretization, we estimate the dynamic potential outcomes by performing the following steps:

1. First, we use the discrete samples $Y_{i,t} = \mathbf{Y}_i(u_t)$, $t = 1, \dots, T$, and construct functional estimators $\hat{\mathbf{Y}}_i$ to approximate the full path-valued \mathbf{Y}_i random variables: with error between each observed sample term $Y_{i,t}$ and estimated population term $\hat{\mathbf{Y}}_i(u_t)$ referred to as *functional estimation error*.
2. Second, the individual estimated functional observations $\hat{\mathbf{Y}}_i^{(x)}$ are used as plug-in estimates for $F(\mathbf{Y}_i^{(x)})$, $i = 1, \dots, n$ in (8) to compute the unique empirical Fréchet mean $F(\hat{\mathbf{Y}}_i^{(x)})$, $i = 1, \dots, n$.

$$F(\hat{\mathbf{Y}}_i^{(x)}), i = 1, \dots, n = \arg \min_{f \in \mathcal{F}} \sum_{i=1}^n \phi^2(f, \hat{\mathbf{Y}}_i^{(x)}). \quad (12)$$

The functional estimation error can be bounded if we assume the metric ϕ is Lipschitz (e.g., L_2 and Fisher–Rao), the data is bounded and the functional estimator has \sqrt{n} -convergence:

$$\begin{aligned} \sup_{t=1, \dots, T} \left| F(\hat{\mathbf{Y}}_i^{(x)}, i=1, \dots, n)(u_t) - F(\mathbf{Y}_i^{(x)}, i=1, \dots, n)(u_t) \right| &\leq \sup_{i=1, \dots, n} \left| \phi^2(f, \hat{\mathbf{Y}}_i^{(x)}) - \phi^2(f, \mathbf{Y}_i^{(x)}) \right| \\ &\leq 2C_1(\mathcal{F}, \phi) \sup_{i=1, \dots, n} \left\| \hat{\mathbf{Y}}_i^{(x)} - \mathbf{Y}_i^{(x)} \right\|_{\phi} \\ &\leq \frac{1}{\sqrt{T}} \cdot C_2(\mathcal{F}, \phi) \end{aligned} \quad (13)$$

where the constants $C_1(\mathcal{F}, \phi)$ and $C_2(\mathcal{F}, \phi)$ depend only on the underlying metric space, and the last line follows from the assumption that the functional estimator has \sqrt{T} -convergence. Intuitively, as the discretization becomes denser, the functional estimators $\hat{\mathbf{Y}}_i^{(x)} \rightarrow \mathbf{Y}_i^{(x)}$ and hence ensures $\sup_{i=1, \dots, n} \left\| \hat{\mathbf{Y}}_i^{(x)} - \mathbf{Y}_i^{(x)} \right\|_{\phi} \rightarrow 0$.

3.2 Convergence and Consistency for Causal Estimators

Our main focus in this work is on discretized samples $\mathbf{Y}_i \in \mathbb{R}^T$, while also considering a limited infinite-dimensional setting where $\mathbf{Y}_i^{(x)}$ belongs to a Hilbert subspace $\mathcal{H}_Y \subset L_2(\mathcal{F}, \eta_x)$. For finite-dimensional outcomes and Fréchet means computed under the squared Euclidean distance loss ($\phi = \|\cdot, \cdot\|$), these estimators are M -estimators with well-documented consistency and uniform laws of large numbers (van de Geer, 2000). This approach allows us to approximate the potential outcome $F(\mathbf{Y}^{(x)})$ from observed discretized samples $\mathbf{Y}_i \in \mathcal{F}$ by computing an empirical Fréchet mean over finitely many observed points $Y_{i,t}$ on a fixed grid $\{u_t\}_{t=1}^T \subset [0, 1]$. Specifically, for $x \in \{0, 1\}$, we establish the following convergence results:

$$\begin{aligned} F(\hat{\mathbf{Y}}_i^{(x)}, i=1, \dots, n) &\xrightarrow{T \rightarrow \infty} F(\mathbf{Y}_i^{(x)}, i=1, \dots, n) + O\left(\frac{1}{\sqrt{T}}\right) \quad (\text{by (13)}), \\ F(\mathbf{Y}_i^{(x)}, i=1, \dots, n) &\xrightarrow{n \rightarrow \infty} F(\mathbf{Y}^{(x)}) \quad (\text{by ULLN}). \end{aligned}$$

Therefore, in what follows, we will primarily consider $F(\hat{\mathbf{Y}}_i, i=1, \dots, n)$, since it operates on the computationally tractable finite-dimensional representation space \mathbb{R}^T , which is sampled from n realizations of \mathbf{Y}_i .

We also consider a more challenging case where the Fréchet mean estimators are defined under the Fisher–Rao metric, which requires constraining the domain \mathcal{F} of the outcomes \mathbf{Y} . In the infinite-dimensional setting, assuming that outcomes lie in a Hilbert subspace of $L_2([0, 1])$, the uniqueness of the Fréchet mean has been well studied (Bridson and Haefliger, 2013). However, laws of large numbers under different metric choices ϕ are beyond the scope of our work. We direct the reader to Sturm (2003) and Afsari (2011) for further discussion on this topic.

3.2.1 Euclidean Space Outcomes

To illustrate our main results, suppose now that the population measures reside in \mathbb{R}^T equipped with the Euclidean distance $\phi = \|\cdot, \cdot\|$. In general, the asymptotic normality of estimation residuals does not carry over arbitrary distance functions ϕ , but in the Euclidean case we can define the pointwise estimated treatment effect in \mathbb{R}^T :

Definition 3. For random variables $\mathbf{Y}^{(0)}$ and $\mathbf{Y}^{(1)}$ with independent distributions η_0 and η_1 respectively, and taking values in \mathbb{R}^T , assume further that \mathcal{F} is also endowed with a vector space

structure. We can define the *dynamic average treatment function effect* as the estimated pointwise difference:

$$\Delta(t) = F(\mathbf{Y}^{(1)})(t) - F(\mathbf{Y}^{(0)})(t), \quad t = 1, \dots, T \quad (14)$$

The quantity $\Delta \in \mathcal{F}$ captures the *dynamic* (pointwise) difference between the Fréchet means. The scalar φ^{dATE} is recovered from the vector norm:

$$\varphi^{dATE} = \phi(F(\mathbf{Y}^{(1)}), F(\mathbf{Y}^{(0)})) = \|\Delta\|_\phi. \quad (15)$$

In the case of Euclidean distance ϕ , the norm above is simply $\varphi^{dATE} = \|\Delta\|_2$. This leads to the following result:

Theorem 4. *Assuming $\mathbf{Y}^{(1)}$ and $\mathbf{Y}^{(0)}$ are identifiable (Assumptions 1, and 2), and associated with independent distributions η_0 and η_1 , over finite \mathbb{R}^T . Then, the residuals between the effect $\Delta = (\Delta(1), \dots, \Delta(T))^T$ and the pointwise estimator for effect $\hat{\Delta} \in \mathbb{R}^T$ are asymptotically normal:*

$$\sqrt{n}(\hat{\Delta} - \Delta) \xrightarrow{d} \mathcal{N}(\mathbf{0}, \mathbf{K}),$$

where $\mathbf{K} = \mathbb{E}[\Delta\Delta^T]$ reflects the covariance structure of the expected effect. For non-zero population effect $\|\Delta\|_2 > 0$, we further get

$$\sqrt{n}(\hat{\varphi}^{dATE} - \varphi^{dATE}) = \sqrt{n}(\|\hat{\Delta}\|_2 - \|\Delta\|_2) \xrightarrow{d} \mathcal{N}(0, \sigma^2),$$

where

$$\sigma^2 = \frac{1}{\|\Delta\|_2^2 (\|\zeta^{(1)}\Delta\|_2^2 + \|\zeta^{(0)}\Delta\|_2^2)}.$$

and each $\zeta^{(x)}$ being the covariance operator associated with mean-zero Gaussian process characterizing the “limiting fluctuation” of the empirical distribution around the true distribution of $\mathbf{Y}^{(x)}$. Under a zero vector population effect assumption $\|\Delta\|_2 = 0$ we get

$$\sqrt{n}(\hat{\varphi}^{dATE} - \varphi^{dATE}) = \sqrt{n}\|\hat{\Delta}\|_2 \xrightarrow{d} \|\mathcal{Z}\|,$$

where \mathcal{Z} is a mean zero Gaussian vector in \mathbb{R}^T with covariance matrix \mathbf{K} ; the distribution of $\|\mathcal{Z}\|^2$ is a generalized χ^2 -distribution.

Proof. See Appendix C.1. □

Remark 5. The pointwise residuals are also asymptotically normal with:

$$\sqrt{n}(\hat{\Delta}(t) - \Delta(t)) \xrightarrow{d} \mathcal{N}(0, K_t), \quad t = 1, \dots, T$$

where $K_t = \mathbb{E}[\Delta(t)^2]$.

Remark 6. The asymptotic distribution of the residuals allows us to derive closed form confidence intervals under both scenarios. For strictly positive norms $\varphi^{dATE} > 0$, a $(1 - \alpha)$ confidence interval (CI) for $\|\Delta\|_2$ is:

$$\text{CI: } \left[\hat{\varphi}^{dATE} - z_{\alpha/2} \sqrt{\frac{\hat{\sigma}^2}{n}}, \hat{\varphi}^{dATE} + z_{\alpha/2} \sqrt{\frac{\hat{\sigma}^2}{n}} \right],$$

where $\hat{\sigma}^2$ is an estimator of σ^2 , obtained by substituting $\hat{\Delta}$ for Δ in the variance formula. The asymptotic normality of a doubly robust version of Δ was also recently proven in [Testa et al. \(2025\)](#).

If we relax the assumptions to include $\varphi^{dATE} > 0$ zero norm assumption, we can write the confidence interval in terms of the spectral decomposition of \mathcal{K} ($\|\mathcal{Z}\|_2 = \sqrt{\sum_{i=1}^T \lambda_i Y_i^2}$, with λ_i as the eigenvalues of \mathcal{K} and $Y_i \stackrel{\text{iid}}{\sim} \mathcal{N}(0, 1)$). A $(1 - \alpha)$ confidence interval (CI) for $\|\Delta\|_2$ is:

$$\text{CI: } \left[\frac{\chi_{T, \alpha/2} \cdot \sqrt{\sum_{i=1}^T \lambda_i}}{\sqrt{n}}, \frac{\chi_{T, 1-\alpha/2} \cdot \sqrt{\sum_{i=1}^T \lambda_i}}{\sqrt{n}} \right],$$

where $\chi_{T, \alpha/2}$ and $\chi_{T, 1-\alpha/2}$ are the lower and upper $\alpha/2$ quantiles of the χ_T distribution.

3.2.2 Fisher–Rao Structured Outcomes

An important but more challenging scenario is when we assume that path-valued $\mathbf{Y}_i \in \mathbb{R}^T$ are observed with flexibility or domain warping along the x -axis. This can impact how well-aligned functions are, which affects the properties of the resulting Fréchet mean estimators for the potential outcomes $F(\hat{\mathbf{Y}}^{(x)})$, as well as the computation of the scalar estimator $\hat{\varphi}^{dATE}$. Account for possible domain warping requires adopting more complex distance measures ϕ . Motivated by common assumptions in *elastic functional data analysis*, we consider the case where the underlying population-level outcomes \mathbf{Y}_i are assumed to be continuous functions, i.e., elements of the metric space (\mathcal{F}, ϕ) , where $\mathcal{F} = C(\mathcal{T})$ for a vector domain \mathcal{T} . We endow \mathcal{F} with the Fisher–Rao metric ϕ , as use of the Euclidean metric on L_2 space may not be a suitable representation space for such functions ([Srivastava et al., 2011](#)). This metric is commonly used to align (or register) functions by estimating their phase variabilities relative to each other; this is because the Fisher–Rao metric is invariant to domain warpings (i.e., reparameterization).

Let

$$\Gamma = \{\gamma : [0, 1] \rightarrow [0, 1] \mid \gamma(0) = 0, \gamma(1) = 1, \text{ and } \gamma \text{ is an orientation-preserving diffeomorphism}\}$$

be the space of all possibly nonlinear domain warpings. Then applying $\gamma \in \Gamma$ to any function $\mathbf{Y}_i \in \mathcal{F}$ yields a reparameterization $\mathbf{Y}_i \circ \gamma$. Invariance to domain warpings means that for all $\gamma \in \Gamma$, $f \in \mathcal{F}$, and $\eta_1, \eta_2 \in T_f(\mathcal{F})$,

$$\langle\langle \eta_1 \circ \gamma, \eta_2 \circ \gamma \rangle\rangle_{f \circ \gamma} = \langle\langle \eta_1, \eta_2 \rangle\rangle_f.$$

The Fisher–Rao metric ϕ defined as:

$$\phi(\mathbf{Y}_i, f) = 2 \arccos \left(\sum_{j=1}^T \sqrt{Y_{i,j} f_j} \right).$$

While this is a complex Riemannian metric, its computation and induced geometry is vastly simplified by defining the *square-root slope function (SRSF)* transformation of function $f \in \mathcal{F}$: $q(t) = \text{sign}(\dot{f}(t)) \sqrt{|\dot{f}(t)|}$. It has been shown that under this transformation, the Fisher–Rao metric reduces to the Euclidean metric on L_2 : in other words, it can be computed by the Euclidean metric between SRSF-transformed functions. Substituting the Fisher–Rao metric in [\(10\)](#) leads to an expression for the potential outcome $\mathbb{E}\{\mathbf{Y}^{(x)} \mid \mathbf{V}\}$ using the Fréchet mean $F(\mathbf{Y}^{(x)})$ measure of

central tendency:

$$\mathbb{E} \left\{ \mathbf{Y}^{(x)} \mid \mathbf{V} \right\} = \arg \min_{\hat{f}} \sum_{i: X_i=x} \left(\int_0^1 \left(\text{sign}(\hat{f}(t)) \sqrt{|\hat{f}(t)|} - \frac{\text{sign}(\dot{Y}_{i,t}) \sqrt{|\dot{Y}_{i,t}|}}{\pi(\mathbf{V})} \right)^2 dt \right). \quad (16)$$

which is not available in closed form and we have used $\pi(\mathbf{V}) = p(X = x | \mathbf{V})$. We have used $\dot{Y}_{i,t}$ to denote the derivative of the observed \mathbf{Y}_i across each dimension after appropriate smoothing, interpolation and scaling made to estimate the population absolutely continuous functions on $[0, 1]$. The resulting optimization problem in (16) is computationally challenging but can be efficiently addressed using the square-root slope function of the original \mathbf{Y}_i and we summarize a practical algorithm in Appendix B. We note that in practice, observations used for computing the SRSF transform are only available as discretized samples in \mathbb{R}^T from these continuous trajectories.

The Fisher–Rao metric is not necessarily convex in \mathbb{R}^T , limiting some of our results for the more constrained vector domain \mathcal{T} . We proceed by stating restricted domain assumptions for the space \mathcal{F} , which still facilitate strong consistency results for the empirical Fréchet mean estimators of the potential outcomes $F(\mathbf{Y}^{(x)})$. To ensure the monotonicity constraints required by our analysis, we consider a subset $\mathcal{T} \subset \mathcal{D} \subset \mathbb{R}^T$. Consequently, we focus on functions that are bounded over \mathcal{T} . Formally, we restrict our original space \mathcal{F} to

$$\mathcal{G} = B(\mathcal{T}) \subseteq \mathcal{F},$$

the space of bounded functions on \mathcal{T} . Likewise, we restrict the pushforward measure η_x to \mathcal{G} , obtaining a new measure P_x defined by

$$P_x(A) = \eta_x(A \cap \mathcal{G}) \quad \text{for all measurable sets } A \subseteq \mathcal{G}.$$

In other words, P_x is a more specialized (conditional) version of η_x , supported only on those functions in \mathcal{F} that lie in \mathcal{G} . Throughout the remainder of our analysis, we work with this pair (\mathcal{G}, P_x) and endow \mathcal{G} with the Fisher–Rao metric ϕ , as required for our result below.

Theorem 7. *Consider the domain*

$$\mathcal{D} = \{ \mathbf{Y} = (Y(1), \dots, Y(T))^\top \in \mathbb{R}^T \mid Y(1) < \dots < Y(T) \} \subset \mathbb{R}^T,$$

and define

$$\mathcal{T} = \mathcal{D} \cap \left[0, \frac{1}{T} - \frac{\delta}{T} \right]^T \subset \mathbb{R}^T,$$

for some small $\delta > 0$ with $1/T > \delta$. Suppose we observe n outcomes $\mathbf{Y}_1, \mathbf{Y}_2, \dots, \mathbf{Y}_n \in \mathcal{T}$, each written as $\mathbf{Y}_i = (Y_i(1), \dots, Y_i(T))^\top \in \mathcal{T}$. These arise from objects $f_i \in \mathcal{G}$ via sampling scheme $f_i \sim P_x$, where P_x is a probability measure defined on the finite T -dimensional metric space (\mathcal{G}, ϕ) with $\mathcal{G} = B(\mathcal{T})$ consisting of bounded functions on \mathcal{T} and ϕ a Fisher–Rao metric.

(1) *Population Fréchet mean in \mathcal{G} . The unique (by Assumption 3) population Fréchet mean of $\{f_i\}_{i=1}^n$ in \mathcal{G} with respect to Fisher–Rao metric is*

$$\bar{f} = \arg \min_{g \in \mathcal{G}} \sum_{i=1}^n \phi(f_i, g)^2 = \arg \min_{g \in \mathcal{G}} \sum_{i=1}^n \left(2 \arccos \left(\int_0^1 \sqrt{f_i(t) g(t)} dt \right) \right)^2. \quad (17)$$

(2) *Sample-level empirical Fréchet mean in $\mathcal{T} \subset \mathbb{R}^T$. Define the map*

$$\phi(\mathbf{Y}_i, \mathbf{g}) = 2 \arccos \left(\sum_{j=1}^T \sqrt{Y_i(j) g_j} \right),$$

for $\mathbf{g} = (g_1, \dots, g_T) \in \mathcal{T}$. Then the empirical Fréchet mean over the observed points $\{\mathbf{Y}_i\}_{i=1}^n$ with respect to Fisher–Rao metric is

$$\bar{f}_n = \arg \min_{\mathbf{g} \in \mathcal{T}} \frac{1}{n} \sum_{i=1}^n \phi(\mathbf{Y}_i, \mathbf{g})^2 = \arg \min_{\mathbf{g} \in \mathcal{T}} \frac{1}{n} \sum_{i=1}^n \left[2 \arccos \left(\sum_{j=1}^T \sqrt{Y_i(j) g_j} \right) \right]^2. \quad (18)$$

(3) *Uniqueness and convergence.* Assume that the minimizer in (18), $\mathbf{g}_* \in \mathcal{T}$, is not of the form $k \cdot \mathbf{1}$ for any constant $k \in \mathbb{R}$. Under condition (1) to (3) and suitable regularity conditions on ϕ and on the data-generating process), \bar{f}_n converges to the unique solution of

$$\inf_{\mathbf{g} \in \mathbb{R}^T} \frac{1}{n} \sum_{i=1}^n \phi(\mathbf{Y}_i, \mathbf{g}),$$

as $n \rightarrow \infty$. Hence, the \bar{f}_n behaves as a Huber-type ρ -estimator in the sense that it is defined via a sample-based loss minimization with consistent and (under non-degeneracy) unique solutions, even though ϕ is not necessarily convex in \mathbb{R}^T .

Proof. See Appendix C.2. □

Corollary 8. Denote the expectation $\mathbb{E}_{P_x} \bar{f}$ in (17) as $\lambda(\mathbf{g})$, $\mathbf{g} \in \mathbb{R}^T$ treated as a finite-dimensional parameter, and assume that $\frac{\partial \lambda}{\partial \mathbf{g}} \big|_{\mathbf{g}=\bar{f}}$ is not degenerated at \bar{f} and have derivative matrix $\mathbf{\Lambda}$. Then, $\sqrt{n}(\bar{f}_n - \bar{f})$ is asymptotically normal with mean zero and covariance $\mathbf{\Lambda}^{-1} \mathbf{C} \mathbf{\Lambda}^{-\top}$ where \mathbf{C} is the covariance matrix of $\phi(\mathbf{Y}, \bar{f})$ under the sampling scheme $f_i \sim P_x$.

Proof. Since \bar{f}_n is a Huber-type ρ -estimator from our previous theorem, we apply Theorem 6.6 of Huber and Ronchetti (2011) or corresponding result in Huber (1967), follows. □

4 Kernel-based Inference of Causal Effects

In this section, we extend kernel-based estimation (Singh et al., 2020) to time path outcomes, formulating closed-form kernel estimators for causal effect functions. These estimators leverage the dependence structure in the outputs for efficient estimation while avoiding explicit point-wise propensity score computation. As shown by Singh et al. (2020), defining the functional that maps heterogeneous response curves to discrete realizations in an RKHS allows for bounded representations, resolving key challenges in nonparametric causal function estimation with continuous treatments.

Building on this, we construct kernel estimators for dynamic heterogeneous treatment effects and extend them to dose-response settings, accommodating both continuous treatments $x \in \mathbb{R}^+$ and path-valued outcomes or covariates. To further generalize these estimators, we incorporate results from operator-valued kernels (Kadri et al., 2016), enabling direct estimation of causal effects from function-valued covariates and outcomes. Additionally, leveraging techniques from elastic functional data analysis, we introduce an iterative alignment scheme for functional covariates and outcomes, enhancing kernel-based estimation of causal quantities such as the average treatment effect, dose-response, and heterogeneous dose-response, particularly in the presence of misaligned functional covariates and outcomes across subjects.

This framework seamlessly integrates both function-valued (infinite-dimensional) and vector-valued (\mathbb{R}^T) representations, providing a unified approach to kernel-based causal inference across diverse outcome spaces.

4.1 Vector-Valued Kernel Estimators

Singh et al. (2020) show that by defining the relevant causal functionals in a reproducing kernel Hilbert space (thereby ensuring their boundedness and resolving technical issues with continuous treatments), the estimation of causal parameters such as φ^{ATE} , φ^{CATE} , and φ^{DS} can indeed be cast as a nonparametric RKHS regression problem for scalar outcomes and vector covariates. One of the main practical advantages of this approach is that it does not require explicit estimation of the propensity function $\pi(\mathbf{V}) = p(X = x \mid \mathbf{V} = \mathbf{v})$. In the continuous-treatment setting, this function is sometimes called the *generalized propensity score*, and while it can be estimated in the literature (see, e.g., Imai and Van Dyk, 2004), it is subject to potential model misspecification and can be difficult to estimate accurately, especially if one does not impose strong parametric assumptions.

Denote the reproducing kernel Hilbert spaces (RKHS) $\mathcal{H}_{\mathcal{X}}$ and $\mathcal{H}_{\mathcal{V}}$ associated with kernels $k_{\mathcal{X}}$ and $k_{\mathcal{V}}$ respectively. Define the feature maps:

$$\begin{aligned}\psi_{\mathcal{X}} : \mathcal{X} &\rightarrow \mathcal{H}_{\mathcal{X}}, & x_i &\mapsto \psi_{\mathcal{X}}(x_i), \\ \psi_{\mathcal{V}} : \mathcal{V} &\rightarrow \mathcal{H}_{\mathcal{V}}, & \mathbf{v}_i &\mapsto \psi_{\mathcal{V}}(\mathbf{v}_i).\end{aligned}$$

The feature maps $\psi_{\mathcal{X}}$ and $\psi_{\mathcal{V}}$ “collect” the points x_i and \mathbf{v}_i mapping them from discrete sample points into their corresponding RKHS. If we denote the true regression $f \in \mathcal{H}_{\mathcal{X} \times \mathcal{V}}$ of the expected outcomes given treatment and covariates defined on $\mathcal{X} \times \mathcal{V}$, by the reproducing property, for any $(x, \mathbf{v}) \in \mathcal{X} \times \mathcal{V}$,

$$f(x, \mathbf{v}) = \langle f, \psi_{\mathcal{X}}(x) \otimes \psi_{\mathcal{V}}(\mathbf{v}) \rangle_{\mathcal{H}_{\mathcal{X} \times \mathcal{V}}}, \quad (19)$$

where \otimes denotes the tensor (or Kronecker) product, and $\langle \cdot, \cdot \rangle_{\mathcal{H}_{\mathcal{X} \times \mathcal{V}}}$ denotes the inner product in the RKHS $\mathcal{H}_{\mathcal{X} \times \mathcal{V}}$. Analogously, we can estimate the expected potential outcome $\mathbb{E}[Y^{(x)} \mid X = x, \mathbf{V} = \mathbf{v}]$ nonparametrically: if we assume the usual *no unmeasured confounding*, the typical integral involved in estimating $\mathbb{E}[Y^{(x)} \mid X = x, \mathbf{V} = \mathbf{v}]$ (i.e., (1)) takes the form of the inner product:

$$\varphi(x, \mathbf{v}) = \langle \varphi, \psi_{\mathcal{X}}(x) \otimes \mu_{\mathbf{v}} \rangle_{\mathcal{H}}, \quad \text{with } \mu_{\mathbf{v}} = \int \psi(\mathbf{v}) dP_{\mathbf{V}}(\mathbf{v}). \quad (20)$$

For sub-population specific (i.e., potential outcome for previously exposed to strata $ox\ x$) or conditional (i.e., strata of \mathbf{v} determined by additional covariates) causal effects, one would change the integrating measure $P_{\mathbf{V}}(\mathbf{v})$ from a marginal over the covariates to an appropriate conditional.

Building on this framework, consider the outcomes are discretized samples from functions representing the outcomes $\mathbf{Y} = (\mathbf{Y}(u_1), \dots, \mathbf{Y}(u_T)) \in \mathbb{R}^T$. Following this, we adopt the convention:

$$\mathbf{Y} = \begin{pmatrix} \mathbf{Y}_1(u_1) & \cdots & \mathbf{Y}_1(u_T) \\ \vdots & & \vdots \\ \mathbf{Y}_n(u_1) & \cdots & \mathbf{Y}_n(u_T) \end{pmatrix} \in \mathbb{R}^{n \times T}, \quad \text{vec}(\mathbf{Y}) = \begin{pmatrix} \mathbf{Y}_1(u_1) \\ \vdots \\ \mathbf{Y}_1(u_T) \\ \vdots \\ \mathbf{Y}_n(u_1) \\ \vdots \\ \mathbf{Y}_n(u_T) \end{pmatrix} \in \mathbb{R}^{nT \times 1}.$$

Although this effectively treats each functional curve \mathbf{Y}_i as a T -dimensional vector (which can have drawbacks; see Ramsay and Silverman, 2005), it is conceptually simple and directly compatible with standard RKHS techniques for vector-valued kernels. Let denote $k_{\mathcal{X} \times \mathcal{V}} : (\mathcal{X} \times \mathcal{V}) \times (\mathcal{X} \times \mathcal{V}) \rightarrow \mathbb{R}$ the separable kernel defined by $k_{\mathcal{X} \times \mathcal{V}}((x, v), (x', v')) = k_{\mathcal{X}}(x, x') k_{\mathcal{V}}(v, v')$. Denote by $\mathbf{K}_{\mathcal{XV}} \in$

$\mathbb{R}^{n \times n}$ the associated Gram matrix evaluated on the training data $\{(x_i, v_i)\}_{i=1}^n$ with $(\mathbf{K}_{XV})_{ij} = k((x_i, v_i), (x_j, v_j))$. To capture dependencies among the T outputs in each functional curve, let $\mathbf{K}_Y \in \mathbb{R}^{T \times T}$ encode the correlation structure among measurement points (e.g., time dependence u_1, \dots, u_T). We then form a Kronecker-structured kernel on $\mathcal{X} \times \mathcal{V}$ with multi-dimensional output:

$$\mathbf{K}_{XX} = \mathbf{K}_{XV} \otimes \mathbf{K}_Y \in \mathbb{R}^{nT \times nT},$$

see [Luo and Strait \(2024\)](#) for kernel methods designed to incorporate more advanced between-curve dependence. Assuming we have n samples $\{\mathbf{v}_i\}_{i=1}^n$ from the distribution of \mathbf{V} , we can approximate the point-wise expected potential outcomes $\mathbb{E}\{\mathbf{Y}^{(x)}|\mathbf{V}\}$ via averaging over $\hat{\varphi}(x, \mathbf{v})$:

$$\hat{\varphi}(x) = \frac{1}{n} \sum_{i=1}^n \hat{\varphi}(x, \mathbf{v}_i) = \frac{1}{n} \sum_{i=1}^n \mathbf{K}_{(x, \mathbf{v}_i)X} (\mathbf{K}_{XX} + \lambda \mathbf{I}_{nT})^{-1} \text{vec}(\mathbf{Y}). \quad (21)$$

Alternatively, we can also represent the expected potential outcome estimator over average covariate values in terms of the average kernel:

$$\hat{\varphi}(x) = \bar{\mathbf{K}}_{xX} (\mathbf{K}_{XX} + \lambda \mathbf{I}_{nT})^{-1} \text{vec}(\mathbf{Y}), \quad (22)$$

where $\bar{\mathbf{K}}_{xX} = \frac{1}{n} \sum_{i=1}^n \mathbf{K}_{(x, \mathbf{v}_i)X}$ and

$$\mathbf{K}_{(x, v), X} = \underbrace{[k((x, v), (x_1, v_1)), \dots, k((x, v), (x_n, v_n))]_{\in \mathbb{R}^{1 \times n}}}_{\in \mathbb{R}^{T \times T}} \otimes \underbrace{\mathbf{K}_Y}_{\in \mathbb{R}^{T \times T}} \in \mathbb{R}^{T \times nT}.$$

Given a new input (x, \mathbf{v}) , the predicted T -dimensional response is

$$\hat{\varphi}(x, \mathbf{v}_j)^{new} = \mathbf{K}_{(x, \mathbf{v}_j)X} \hat{\varphi}(x) \in \mathbb{R}^T.$$

This construction exploits both input similarity (via \mathbf{K}_{XV}) and the output dependence structure (via \mathbf{K}_Y) in a unified kernel ridge regression framework. In Bayesian extensions, one may require additional conditions on the kernels (e.g., nuclear dominance [Chau et al., 2021](#), non-stationary kernels [Noack et al., 2024](#) or low-rank assumptions [Luo et al., 2022](#)) or spectral representations of the Hilbert space ([Dance et al., 2024](#)).

Recall that $\hat{\varphi}(x)$ becomes our kernel estimator for (12) from above. To recover expressions for estimators for the point-wise binary treatment effect $\hat{\Delta}(t)$, the scalar $\hat{\varphi}^{dATE}$ and the continuous treatment extension $\hat{\varphi}^{dDS}(x)$, we compute:

$$\hat{\Delta}(t) = \hat{\varphi}(1)(t) - \hat{\varphi}(0)(t), \quad t = 1, \dots, T \quad (\text{Pointwise binary effect}) \quad (23)$$

$$\hat{\varphi}^{dATE} = \|\hat{\varphi}(1) - \hat{\varphi}(0)\|_{\phi} \quad (\text{Dynamic binary treatment effect}) \quad (24)$$

$$\hat{\varphi}^{dDS} = \|\hat{\varphi}(x)\|_{\phi} \quad (\text{Dynamic dose response}) \quad (25)$$

4.2 Operator-Valued Kernel Estimators

In the previous subsection, we discretized the functional outcomes into \mathbb{R}^T and employed a multi-output kernel approach. While conceptually straightforward, such methods rely on a finite grid of points and do not directly accommodate *registration* or *alignment* in a single framework, which may be desirable if functions are misaligned with respect to their domains. To address this, we now consider operator-valued kernels [Kadri et al. \(2016\)](#), which generalize real- or matrix-valued kernels to the fully functional setting by mapping from (possibly) functional inputs to bounded linear operators acting on a Hilbert space of functional outputs. This viewpoint supports curve

registration via kernel design, enabling us to model re-parameterizations (e.g., time warping) of the input or output domains in a unified RKHS paradigm (Micchelli et al., 2005).

Let \mathbf{Y}_i be an outcome curve lying in a separable Hilbert space \mathcal{H}_Y (e.g. $L^2(\mathcal{U})$), and keep the notation from above \mathcal{H}_X and \mathcal{H}_V describing the corresponding RKHS for the treatment and covariates (the input covariates can be finite and mapped via ψ_V to \mathcal{H}_V or directly elements of \mathcal{H}_V). We need to then further define an operator-valued kernel \mathcal{K} :

$$\mathcal{K} : (\mathcal{H}_X \times \mathcal{H}_V) \times (\mathcal{H}_X \times \mathcal{H}_V) \longrightarrow \mathcal{L}(\mathcal{H}_Y),$$

where $\mathcal{L}(\mathcal{H}_Y)$ is the space of bounded linear operators on \mathcal{H}_Y . For example, we can consider the following operator-valued kernel induced by separable kernel defined on $\mathcal{X} \times \mathcal{V}$:

$$\begin{aligned} \mathcal{K} \left(\underbrace{(X_i, \mathbf{V}_i)}_{N \text{ samples}}, \underbrace{(X_j, \mathbf{V}_j)}_{N \text{ samples}} \right) &= k_X^*(X_i, X_j) \cdot k_V^*(\mathbf{V}_i, \mathbf{V}_j) \cdot k_{\mathcal{H}_Y}, \\ &= k_X^*(X_i, X_j) \cdot k_V^*(\mathbf{V}_i, \mathbf{V}_j) \cdot I_{\mathcal{H}_Y}. \end{aligned} \quad (26)$$

for $I_{\mathcal{H}_Y}$ denoting the identity operator on \mathcal{H}_Y to ensure that the path estimate still lives in \mathcal{H}_Y . (26) assumes that the treatment and covariates are already embedded in their associated Hilbert spaces \mathcal{H}_X and \mathcal{H}_V since $k_X^* : \mathcal{H}_X \times \mathcal{H}_X \rightarrow \mathbb{R}$ and $k_V^* : \mathcal{H}_V \times \mathcal{H}_V \rightarrow \mathbb{R}$ (i.e., otherwise the feature maps ψ_X and ψ_V are further applied). Note that if each \mathbf{V}_i itself is already a function (e.g. $\mathbf{V}_i \in L^2(\mathcal{U})$), the map $\psi_V : \mathcal{V} \rightarrow \mathcal{H}_V$ allows to simply embeds one Hilbert space into another, permitting more specialized notions of functional similarity or alignment.

The regression of the conditional expectation $\mathbb{E}[\mathbf{Y} \mid X, \mathbf{V}]$ from (19) can be extended and by the reproducing property of an *operator-valued* RKHS $\mathcal{H}_{\mathcal{K}}^{\text{op}}$, we write the true regression function as:

$$m(x, \mathbf{v}) = \langle m, \Psi((x, \mathbf{v})) \rangle_{\mathcal{H}_{\mathcal{K}}^{\text{op}}}, \quad \text{with } \Psi : (\mathcal{X} \times \mathcal{V}) \rightarrow \mathcal{H}_{\mathcal{K}}^{\text{op}} \text{ operator-valued feature map.}$$

Consistent with the kernel ridge regression approach in Section 4.1, the estimation of the conditional expectation operator $m : \mathcal{X} \times \mathcal{V} \rightarrow \mathcal{Y}^{\mathbb{E}[\cdot \mid X=x, \mathbf{V}=\mathbf{v}]} \mathbb{R}$, minimizes:

$$\min_{m \in \mathcal{H}_{\mathcal{K}}^{\text{op}}} \sum_{i=1}^n \|\mathbf{Y}_i - m(X_i, \mathbf{V}_i)\|_{\mathcal{H}_Y}^2 + \lambda \|m\|_{\mathcal{H}_{\mathcal{K}}^{\text{op}}}^2$$

where $\lambda > 0$ is a regularization parameter. By the Representer Theorem for operator-valued kernels, the solution m has the form:

$$m(\cdot, \cdot) = \sum_{j=1}^n \mathcal{K}((\cdot, \cdot), (X_j, \mathbf{V}_j)) \alpha_j, \quad (27)$$

where $\alpha_i \in \mathcal{H}_Y$ (i.e., extending to $m(\cdot, \cdot) = \sum_{j=1}^n \mathcal{K}((\cdot, \cdot), (\phi(X_j), \phi(\mathbf{V}_j))) \alpha_j$ for if treatment and covariates need to be first embedded in an appropriate Hilbert space). Substituting \mathcal{K} and simplifying, we have $m(\cdot, \cdot) = \sum_{j=1}^n k_X^*(\cdot, X_j) \cdot k_V(\cdot, \mathbf{V}_j) \cdot \alpha_j$. Let $\boldsymbol{\alpha} = [\alpha_1, \dots, \alpha_n]^\top \in \mathbb{R}^{n \times 1}$ and $\mathcal{K}_{ij} = k_X(X_i, X_j) \cdot k_V(\mathbf{V}_i, \mathbf{V}_j)$, where each $\alpha_i \in \mathcal{H}_Y$. We summarize the optimization inference as:

$$\min_{\boldsymbol{\alpha}} \sum_{i=1}^n \left\| \mathbf{Y}_i - \sum_{j=1}^n \mathcal{K}_{ij} \alpha_j \right\|_{\mathcal{H}_Y}^2 + \lambda \sum_{i,j=1}^n \langle \alpha_i, \mathcal{K}_{ij} \alpha_j \rangle_{\mathcal{H}_Y}.$$

In other words, we can perform a feature estimation using functional data analysis by putting both samples from X_i into $\psi_{\mathcal{X}}(X_i)$; and \mathbf{V}_i into $\psi_{\mathcal{V}}(\mathbf{V}_i)$; \mathbf{Y}_i into $\psi_{\mathcal{Y}}(\mathbf{Y}_i)$.

We can summarize our estimators for potential outcomes in the case when outcomes are elements of the metric space (\mathcal{F}, ϕ) (i.e., and $\mathcal{X} \sim \mathbb{R}$) as an operator $\hat{\varphi}(x) : \mathbb{R} \rightarrow \mathcal{F}$ which integrates the effect of covariates \mathbf{V} from the Fréchet means:

$$\begin{aligned} \hat{\varphi}(x) &= \int_{\mathcal{V}} F(\psi_{\mathcal{Y}}(\mathbf{Y}) | \psi_{\mathcal{V}}(\mathbf{V}), X = x) dP_{\mathbf{V}}(\psi_{\mathcal{V}}(\mathbf{v})) \\ &= \frac{1}{n} \sum_{j=1}^n \mathcal{K}_{(\psi_{\mathcal{X}}(X_*), \psi_{\mathcal{Y}}(\mathbf{Y}_j))}(\psi_{\mathcal{X}}(X), \psi_{\mathcal{V}}(\mathbf{v})) (\mathcal{K} + \lambda I_n)^{-1} \mathbf{Y} \end{aligned} \quad (28)$$

with the probability density $P_{\mathbf{V}}$ appropriately chosen over the functional domain \mathcal{V} . Those can then be substituted in the corresponding expressions for dynamic binary treatment effect and dose response in (23) (i.e., pointwise effects only defined in the context of finite-dimensional grids).

SRSF-based Alignment via Kernel Design. As mentioned earlier, the operator-valued kernels allow us to easily embed curve alignment in our kernel \mathcal{K} . Earlier, in Section 3.2.2, we introduced the Fisher–Rao metric and SRSF-based transform to align (or “warp”) functional data residing in a suitable metric space \mathcal{F} . An intuitive way to do this is to incorporate time-warping or reparameterizations *within* the kernel $k_{\mathcal{H}_Y}$ from (26). First, let us use $d_{\text{FR}}(f, g)$ as a shorthand notation for the Fisher–Rao distance (defined in Section 3.2.2) between $f, g \in \mathcal{F}$ in the metric space \mathcal{F} (i.e., here we further assume a Hilbert space).

Theorem 9. *The function*

$$k_{\text{FR}}(f, g) = \exp(-\zeta d_{\text{FR}}(f, g)^2), \quad \zeta > 0,$$

is a positive-definite kernel on \mathcal{F} .

The intuitive proof can be found Appendix B.2. The outcome similarity between curves $\mathbf{Y}_i, \mathbf{Y}_j \in \mathcal{F}$ can be embedded by extending the operator from (26) to include outcome “similarity” via setting:

$$k_{\mathcal{H}_Y}(\mathbf{Y}_i, \mathbf{Y}_j) = k_{\text{FR}}(\mathbf{Y}_i, \mathbf{Y}_j) I_{\mathcal{H}_Y}. \quad (29)$$

This is the direct analog of the $\exp(-\zeta \|\cdot\|^2)$ kernel in scalar or finite-dimensional output spaces, now applied to the functional outputs $\mathbf{Y}_i, \mathbf{Y}_j$. Multiplying by the identity operator $I_{\mathcal{H}_Y}$ ensures each pair of outputs yields a scalar factor but still returns an element of $\mathcal{L}(\mathcal{H}_Y)$. We finish with a practical implementation of an iterative algorithm for computing our estimator $\hat{\varphi}^{d\text{ATE}}$ for the dynamic binary treatment effect when SRSF transformations are used to iteratively align covariates and outcome in Algorithm 1.

5 Experimental Results

To assess the impact of the proposed methods, we conducted synthetic experiments simulating functional data scenarios where traditional causal inference approaches struggle. These experiments illustrate how the estimators introduced in Sections 3 and 4, including functional treatment effect estimators, alignment techniques, and operator-valued kernels, handle challenges posed by functional outcomes and covariates. We analyze two key scenarios: (1) binary treatment with functional outcomes and (2) continuous treatment with functional co-variates and outcomes which are temporally misaligned.

Algorithm 1 Iterative SRVF based Kernel Causal Effect Estimation

Require: Functional covariates $\{V_i(u)\}_{i=1}^n$, outcomes $\{Y_i(v)\}_{i=1}^n$, treatment $\{X_i\}_{i=1}^n$, metric ϕ , kernel functions $k_{\mathcal{X}}, k_{\mathcal{Y}}, k_{\mathcal{Y}}$, corresponding RKHS maps $\psi_{\mathcal{X}}, \psi_{\mathcal{Y}}$ and $\psi_{\mathcal{Y}}$ regularization parameter $\lambda > 0$, maximum iterations R_{\max} , convergence threshold ϵ .

Ensure: Registered curves $\tilde{V}_i(u), \tilde{Y}_i(v)$; estimated conditional expectation $m(x, v)$; causal effects φ^{dATE} (or φ^{dDS} in the last step).

1: Initialize $\tilde{V}_i^{(0)}(u) = V_i(u), \tilde{Y}_i^{(0)}(v) = Y_i(v)$, and set $r = 0$.

2: **while** $r < R_{\max}$ **or** convergence criterion not met **do**

3: Compute the mean curve μ_V for functional covariates:

$$\mu_V^{(r)} \leftarrow \arg \min_{\mu} \sum_{i=1}^n \phi(\tilde{V}_i^{(r)}, \mu_V)$$

4: Compute the mean curve μ_Y for functional outcomes:

$$\mu_Y^{(r)} \leftarrow \arg \min_{\mu} \sum_{i=1}^n \phi(\tilde{Y}_i^{(r)}, \mu_Y)$$

5: **for** $i = 1, \dots, n$ **do**

6: Align covariates:

$$\tilde{V}_i^{(r+1)}(u) \leftarrow \tilde{V}_i^{(r)}(u) \circ \arg \min_{\gamma \in \Gamma} \phi(\tilde{V}_i^{(r)}, \mu_V^{(r)} \circ \gamma)$$

7: Align outcomes:

$$\tilde{Y}_i^{(r+1)}(v) \leftarrow \tilde{Y}_i^{(r)}(v) \circ \arg \min_{\gamma \in \Gamma} \phi(\tilde{Y}_i^{(r)}, \mu_Y^{(r)} \circ \gamma)$$

8: **end for**

9: Map registered curves into RKHS: $\psi_{\mathcal{X}}(X_i) \in \mathcal{H}_{\mathcal{X}}, \psi_{\mathcal{Y}}(\tilde{Y}_i^{(r+1)}) \in \mathcal{H}_{\mathcal{Y}}, \psi_{\mathcal{V}}(\tilde{V}_i^{(r+1)}) \in \mathcal{H}_{\mathcal{V}}$.

10: Compute the kernel matrix $\mathcal{K}^{(r+1)}$ with its (i, j) -th entry as:

$$\mathcal{K}_{ij}^{(r+1)} \leftarrow k_{\mathcal{X}}(\psi_{\mathcal{X}}(X_i), \psi_{\mathcal{X}}(X_j)) \cdot k_{\mathcal{Y}}(\psi_{\mathcal{Y}}(\tilde{V}_i^{(r+1)}), \psi_{\mathcal{Y}}(\tilde{V}_j^{(r+1)}))$$

11: Solve kernel ridge regression:

$$\alpha^{(r+1)} \leftarrow (\mathcal{K}^{(r+1)} + \lambda I)^{-1} \tilde{Y}^{(r+1)}$$

12: For a new input (x, v) , compute:

$$\hat{m}^{(r+1)}(x, v) \leftarrow \sum_{i=1}^n k_{\mathcal{X}}(\psi_{\mathcal{X}}(x), \psi_{\mathcal{X}}(X_i)) \cdot k_{\mathcal{Y}}(\psi_{\mathcal{Y}}(v), \psi_{\mathcal{Y}}(\tilde{V}_i^{(r+1)})) \cdot \alpha_i^{(r+1)}$$

13: **if** $\|\hat{m}^{(r+1)} - \hat{m}^{(r)}\|_2 < \epsilon$, where the norm is evaluated on the training set of size n **then**

14: **Break.**

15: **end if**

16: **end while**

17: Compute dynamic average treatment effect (dATE):

$$\varphi^{dATE} \leftarrow \frac{1}{m} \sum_{j=1}^m (\hat{m}^{(r+1)}(1, V_j) - \hat{m}^{(r+1)}(0, V_j))$$

5.1 Binary Treatment with Synthetic Data

The first experiment simulates functional outcomes $Y(t)$ generated as time-dependent curves influenced by a binary treatment $X \in \{0, 1\}$ and baseline covariates V . We consider two scenarios:

- Functional outcomes modeled as:

$$Y(t) = \mu_0(t) + \beta_X(t)X + \epsilon(t), \quad (30)$$

where $\mu_0(t)$ represents the baseline curve, $\beta_X(t)$ is the time-varying treatment effect, and $\epsilon(t)$ is independent Gaussian noise.

- Monotonic functional outcomes defined as the cumulative sum of an underlying process $Z(t)$:

$$Z(t) = \mu_0(t) + \beta_X(t)X + \epsilon(t), \quad (31)$$

leading to the observed outcome function:

$$Y(t) = \sum_{\tau=1}^t Z(\tau). \quad (32)$$

In both cases, the function $\beta_X(t) = \sum_{i=1}^3 a \cdot \exp\left(-\frac{(t-c_i)^2}{2w^2}\right)$ is parameterized by a , c_i , and w , where c_i are the centers of three equally spaced peaks, controlling the treatment effect’s amplitude, location, and spread. Both cases also simulate the challenge of temporal misalignment, where the outcome curves $Y(t)$ exhibit random shifts in their peak locations across individuals samples. Covariates V are simulated to correlate with both X and $Y(t)$, introducing realistic confounding structures. Theoretical results from Theorem 7 guarantee the consistency of SRVF-based estimators in the monotonic outcome case. However, we empirically evaluate the performance of different estimators in both scenarios. We compare the following estimators: Inverse Probability Weighting (IPW) ATE estimator Imai and Van Dyk (2004); Doubly Robust ATE estimator; Kernel ATE estimator Singh et al. (2020); proposed Operator Kernel ATE estimator (23); SRVF-based Operator Kernel ATE estimator, which registers path outcomes to their Fréchet mean.

Method	$n = 50$	$n = 100$	$n = 250$
IPW ATE	22.70 (14.93)	23.18 (15.31)	22.64 (15.09)
Doubly Robust ATE	21.74 (14.84)	21.98 (15.10)	21.65 (14.88)
Kernel ATE	22.63 (15.25)	23.14 (15.47)	22.61 (15.10)
Operator Kernel ATE	15.18 (10.50)	15.42 (10.70)	13.32 (9.79)
SRVF Operator Kernel ATE	15.15 (10.32)	15.60 (10.49)	12.65 (9.60)

Table 1: Mean absolute error and standard deviation (in brackets) of causal effect estimators for binary treatment and *monotonic* path outcomes \mathbf{Y} .

For each scenario, we simulate five datasets from the described super-population $\{\mathbf{Y}, X, \mathbf{V}\}$ and evaluate the estimators for sample sizes $n \in \{50, 100, 250\}$. We use squared exponential kernel for the covariate kernel (and outcome kernel in the operator setting), and binary kernel for the treatments as proposed originally in Singh et al. (2020). The kernel parameters for the kernel estimators are set using the *median inter-point heuristic* and the regularization terms are set using hyperparameter grid search optimizing the out-of-sample performance holding 20% of the data for testing. Figures 1 and

Method	$n = 50$	$n = 100$	$n = 250$
IPW ATE	0.88 (0.77)	0.89 (0.77)	0.89 (0.79)
Doubly Robust ATE	0.67 (0.67)	0.68 (0.67)	0.66 (0.70)
Kernel ATE	0.87 (0.78)	0.89 (0.78)	0.89 (0.79)
Operator Kernel ATE	0.65 (0.62)	0.62 (0.60)	0.62 (0.60)
SRVF Operator Kernel ATE	0.65 (0.61)	0.64 (0.58)	0.62 (0.57)

Table 2: Mean absolute error and standard deviation (in brackets) of causal effect estimators for binary treatment and *nonmonotonic* path outcomes \mathbf{Y} .

2 present box plots of ATE estimation errors across simulations, while Tables 1 and 2 summarize mean absolute errors and standard deviations across the time grid. Dynamic estimation errors over time of the pointwise estimators $\Delta(t)$ are shown in Figures 3 and 4, respectively. To estimate standard deviation across time, we first average across simulation datasets for each sample size. Our results indicate that the proposed estimators incorporating outcome structure achieve lower mean absolute errors and reduced standard deviations across the time grid. As expected, the doubly robust ATE achieves lower estimation error for smaller n , even without properly accounting for the outcome structure. Functional alignment further reduces error variance, particularly in more complex outcome scenarios, where it allows to flatten the estimation error across the time-grid.

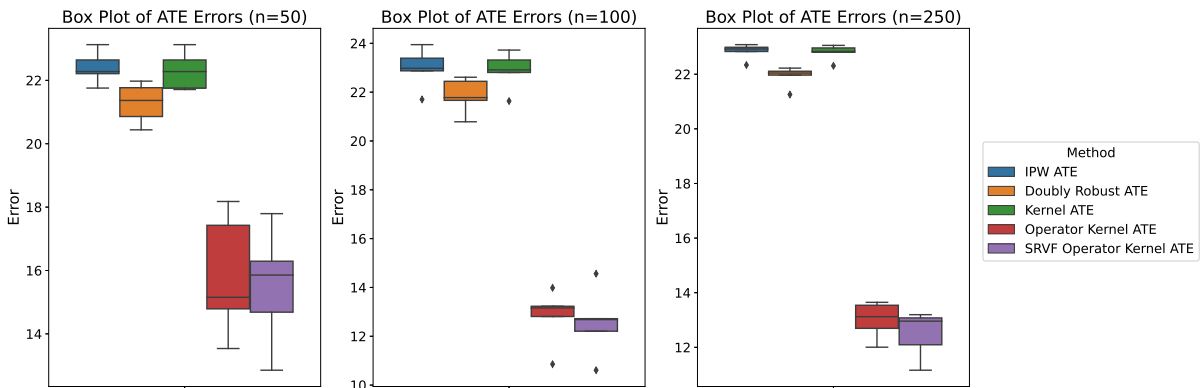


Figure 1: Box plot of ATE estimation errors for *monotonic* path-valued outcomes, across different training sample sizes ($n = 50, 100, 250$). The IPW ATE, Doubly Robust ATE, and Kernel ATE estimators ignore the multivariate structure, whereas the SRVF-based approach accounts for amplitude and phase variability.

5.2 Continuous Treatment with Synthetic Data

The next experiment simulates functional outcomes $Y(t)$ generated as time-dependent curves influenced by a *continuous* treatment $X \in \mathbb{R}$ and time-dependent baseline covariates $V(t)$. Kernel causal estimators (Singh et al., 2020) and our proposed extensions from Section 4 can readily deal with the continuous treatment $X \in \mathbb{R}$ by a simple change of kernel $k_{\mathcal{X}}$ describing the feature maps $\psi_{\mathcal{X}}$. We simulate functional outcomes as:

$$Y(t) = \mu_V(t) + \beta_X(t)X + \epsilon(t), \quad (33)$$

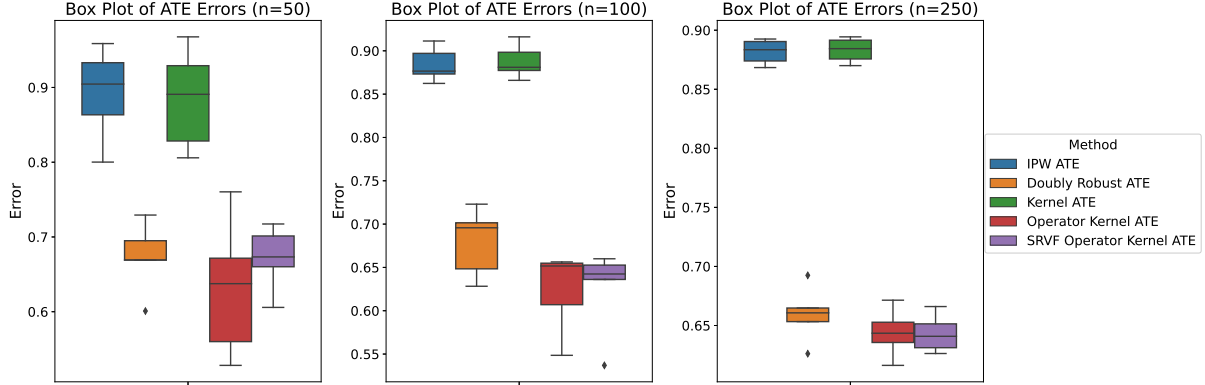


Figure 2: Box plot of ATE estimation errors for *nonmonotonic* path-valued outcomes, across different training sample sizes ($n = 50, 100, 250$). The IPW ATE, Doubly Robust ATE, and Kernel ATE estimators ignore the multivariate structure, whereas the SRVF-based approach accounts for amplitude and phase variability.

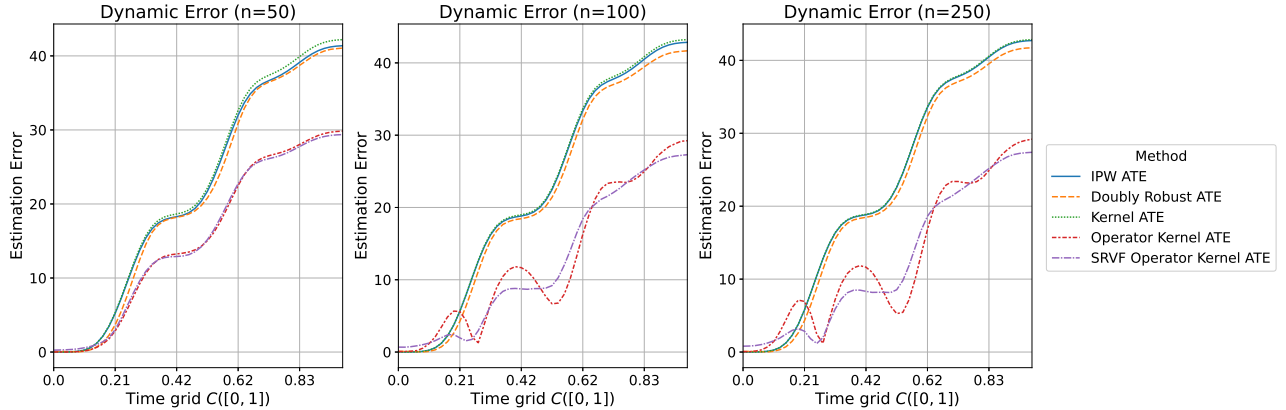


Figure 3: Dynamic error as a function of time for different causal inference estimators for the ATE, assuming *monotonic outcomes*. The plots display the average error (i.e., estimated across 5 draws from the super-population) for varying sample size n .

where $\mu_V(t)$ represents a curve effect (arc parameterized with expected peak location and height) dependent on the covariates, $\beta_X(t)$ is the time-varying treatment effect, and $\epsilon(t)$ is independent Gaussian noise. The function $\beta_X(t) = \sum_{i=1}^3 a \cdot \exp\left(-\frac{(t-c_i)^2}{2w^2}\right)$ is again parameterized by a , c_i , and w , where c_i are the centers of three equally spaced peaks controlling the treatment effect's amplitude, location, and spread. However, in this setup the outcomes are further modulated by time-dependent covariates $V(t)$ which introduce realistic time-dependent confounding. Independent random shifts are introduced in the peak locations for both $Y(t)$ and $V(t)$ across individual samples from the super-population $\{\mathbf{Y}, \mathbf{X}, \mathbf{V}\}$. We compare the different kernel causal effect estimators (Kernel DS estimator as in [Singh et al. \(2020\)](#), proposed Operator Kernel DS estimator (25), and the Iterative SRVF-based Kernel DS estimator) for their mean absolute error in estimating the dose-response effect in the setup of dynamic outcomes and covariates. Mimicking Section 5.1, we simulate five datasets from the described super-population $\{\mathbf{Y}, \mathbf{X}, \mathbf{V}\}$ for the scenarios of sample size $n = 50$,

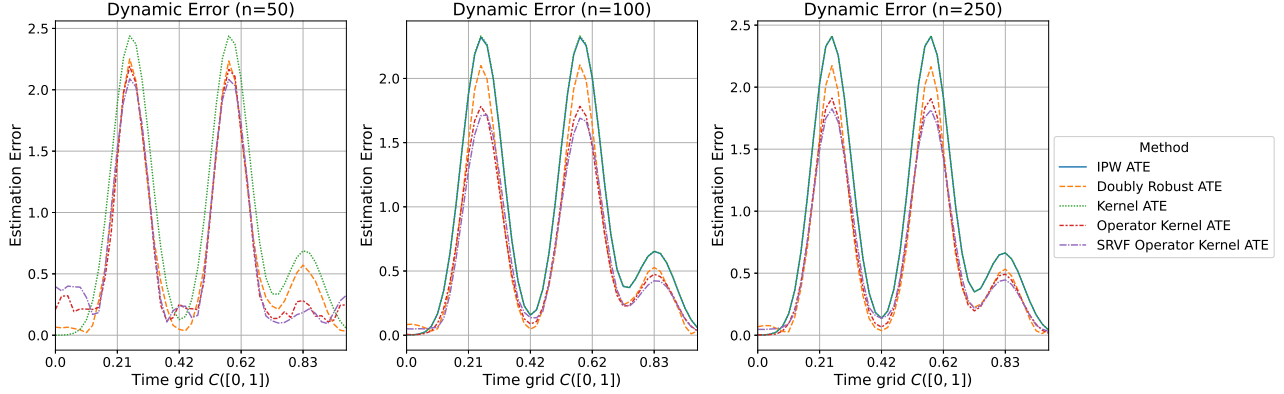


Figure 4: Dynamic error as a function of time for different causal inference estimators for the ATE, assuming *nonmonotonic outcomes*. The plots display the average error (i.e., estimated across 5 draws from the super-population) for varying sample size n .

$n = 100$ and $n = 250$. The squared exponential kernel parameters³ used for covariates and treatment are set using the median inter-point heuristic with regularization terms set using hyperparameter grid search optimizing the out-of-sample performance holding 20% of the data for testing. Figure 5 present a box plot of the DS estimation error across simulations, while Table 3 summarizes the mean absolute error and standard deviation across the time grid. Dynamic estimation errors over time of the pointwise estimators $\Delta(t)$ of the DS are shown in Figures 6. The standard deviation across time is computed over the average estimation error across the simulation datasets for selected sample size.

Our results indicate that isolating and estimating the treatment effects in this more complex scenarios does require more data samples to converge to a robust estimator. The proposed iterative algorithm and operator-valued kernel approach both reduce the standard deviation of the estimation error across the time grid with (i.e., flattens the estimation error) and as we increase the number of samples from $\{\mathbf{Y}, \mathbf{X}, \mathbf{V}\}$ which can be explained with the increase complexity of the effect function (i.e., continuous treatment and time-dependent confounding). Incorporating the outcome structure eventually reduces the error, but requires more samples to achieve a robust estimate.

Method	$n = 50$	$n = 100$	$n = 250$
Kernel DS	0.32 (0.16)	0.32 (0.16)	0.37 (0.16)
Operator Kernel DS	0.33 (0.15)	0.25 (0.15)	0.27 (0.15)
Iterative SRVF Operator Kernel DS	0.30 (0.15)	0.33 (0.16)	0.26 (0.15)

Table 3: Mean absolute error and standard deviation (in brackets) of causal effect estimators for continuous treatment and time-depedent outcomes \mathbf{Y} and covariates \mathbf{V} .

³Replacing the covariates kernel $k_{\mathbf{V}}$ with kernels explicitly designed for sequential data (e.g., the signature kernel Lee and Oberhauser (2023)) would be a sensible approach if we wish to capture more complex temporal features of \mathbf{V} , but we defer this to future work due to the challenges in characterizing the approximation error, convergence properties, and statistical efficiency of using truncated signature features in high-dimensional settings.

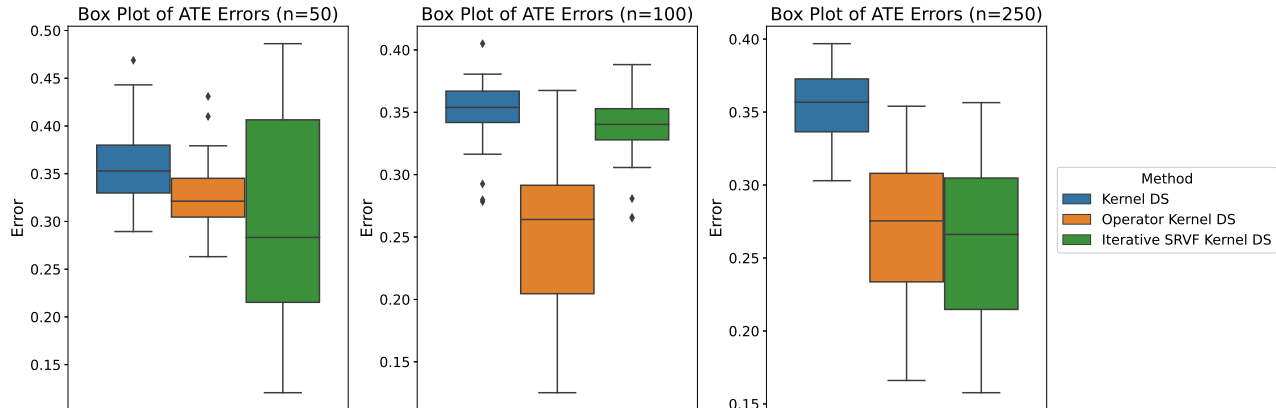


Figure 5: Box plot of DS estimation errors for different methods under continuous treatment and time-dependent confounding, computed across different training sample sizes ($n = 50, 100, 250$). The Kernel DS estimator ignore the multivariate structure, the Operator Kernel DS accounts for the multivariate outcome structure and the Iterative SRVF-based approach also infers the temporal alignment of \mathbf{V} and \mathbf{Y} .

5.3 Causal Effects on Digital Outcomes

Digital biomarkers are increasingly recognized as reliable and sensitive clinical endpoints for assessing disease progression and treatment responses in Parkinson’s disease (PD). The ability to collect near real-time health measurements at scale makes these biomarkers particularly well-suited for functional data analysis. In this section, we apply our proposed framework to estimate the causal effects of (i) resting tremors and (ii) bradykinetic gait on their respective digital outcomes: tremor probability and gait energy. Our analysis is based on data from the Parkinson@Home Validation Study (Evers et al., 2020), which involved two weeks of passive monitoring using a wrist-worn device (Moto 360) in participants with and without PD.

The study included 25 PD patients with motor fluctuations and 25 age-matched non-PD controls. Participants were monitored during both standardized clinical assessments (including MDS-UPDRS Part III) and unscripted daily life activities at home. The PD group underwent two monitoring sessions: once after overnight withdrawal of dopaminergic medication and again one hour post-medication. Additionally, all participants were continuously monitored in free-living conditions for two weeks. For our analysis, we estimate causal effects based on predicted symptom trajectories over this 2-week period.

For PD patients with tremor, we selected data from the most affected arm (determined by MDS-UPDRS Part III, items 3.15 & 3.17). For those without tremor, we selected the corresponding side matched for hand dominance. Due to technical issues with sensor devices in one PD patient and one non-PD control, the final dataset for training symptom detection models included 24 PD patients and 24 controls (further details about the tremor data are available in Evers et al. (2025)). Performance of the trained symptom prediction classifiers is available in Appendix D. Out-of-sample symptom profiles were estimated for:

- 16 PD participants (8 with annotated tremor, 8 without) and 8 age-matched controls to assess the effect of disease status on tremor probability.
- 13 PD participants and 8 age-matched controls to estimate the effect of disease status on gait energy.

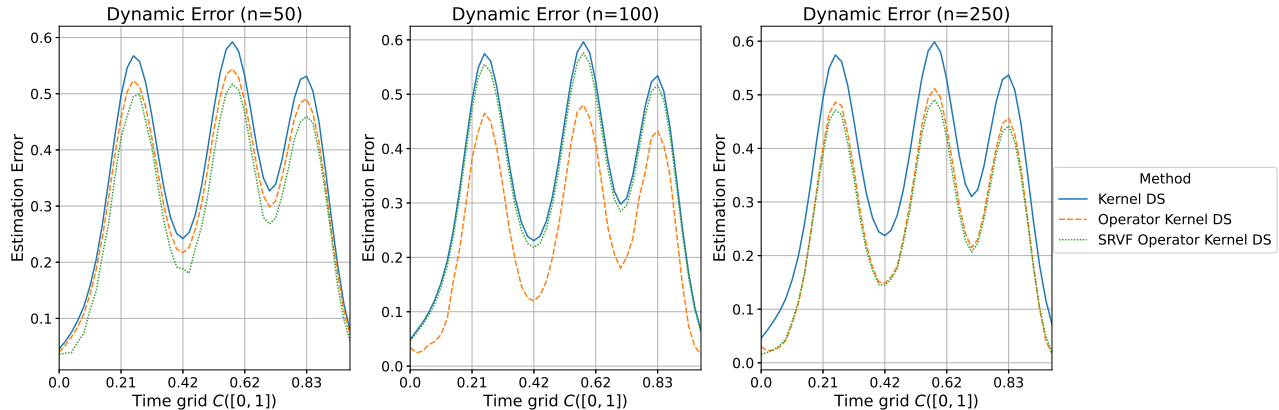


Figure 6: Dynamic error as a function of time for different causal inference estimators for the DS, under continuous treatment and time-dependent confounding. The plots display the average error (i.e., estimated across 5 draws from the super-population) for varying sample size $n = 50, 100, 250$.

For further details on cohort demographics, please refer to Table 4. Based on video recordings, trained research assistants annotated the main activities (e.g., walking, sitting, standing still) and symptoms (e.g., tremor and freezing of gait) occurring during unscripted activities. A movement disorders expert reviewed the symptom annotations. We used tremor presence annotations from the arm with the most severe tremor (i.e., the same side as the accelerometer sensor) and annotations for gait activity. In 8 PD patients, tremor was observed during unscripted daily life activities, whereas in the remaining 16 PD patients, no tremor was observed.

As a first step, we down-sampled the three-axial accelerometer data from the Physilog devices from 200Hz to 50Hz after *anti-aliasing* with a fourth-order moving average filter. To remove the effect of orientation changes of the device, we applied l_1 -trend filtering to each individual axis, assuming piecewise linear changes (Raykov et al. (2020), i.e., setting λ to 10,000). We then segmented the accelerometer data into non-overlapping 5-second windows and extracted features from each axis of the pre-processed accelerometer data (resulting in a total of 84 features for all axes combined, see Appendix D). Following common symptom detection practices, we trained a logistic classifier on home-based video annotations from 48 participants to predict tremor and gait episodes. Classification performance was evaluated against expert annotations and is reported in Table 5. The two classifiers were then used to estimate digital markers reflective of tremor and gait: tremor probability and bout energy during walking, respectively.

These digital markers serve as proxies for symptom severity, allowing us to model their causal relationships with disease status, as outlined in Figure 7. In this figure, we list the causal assumptions regarding known factors expected to affect disease category and the corresponding digital marker.⁴

Effect of PD on Gait Energy First, we quantify the effect of PD on expected gait bout energy during walking periods using 2-week follow-up data from 22 participants (14 PD, 8 non-PD age-matched controls). Gait bouts are predicted out-of-sample via the trained logistic classifier. The 2-week wearable outcomes are averaged to obtain a single daily profile per participant, where outcome curves are smoothed over 15-minute intervals. Daily measurements range between 5 and 12 hours, and the final outcome curves are constructed by aggregating across available days per time bin.

⁴The example presents a simplified version of the problem and does not reflect the full list of factors affecting each digital outcome (e.g., geographic location, disease severity, and other contextual factors).

We model the diagnostic category (binary PD vs. non-PD control) as the intervention variable D while controlling for the confounding effects of *hours awake* and *gender*. Figure 8 presents both the average treatment effect estimated using the IPW estimator and the proposed dATE estimator from Section 5.2. While we observe a strong overlap in potential outcome distributions (z-scored), many PD participants exhibit gait bouts with energy levels indistinguishable from non-PD controls. However, the PD group also displays a higher frequency of low-energy bouts. A Welch t-test on the IPW-estimated distributions fails to reject the null hypothesis that the two gait bout distributions originate from the same population. However, time-specific conditioning, as seen in Figure 11 (Appendix D), reveals significant fluctuations, which are better captured by the dATE estimator (Figure 8) and confirmed by the corresponding Welch t-test. We estimate significant variations in PD gait bout energy, which can be at least partially attributed to dopaminergic therapy (average of four daily levodopa doses among the 14 included PD participants).

Effect of Diagnostic Category on Tremor Next, we quantify the effect of PD tremor diagnosis on expected tremor probabilities using 2-week follow-up data from 24 participants (8 PD with annotated tremor, 8 PD without annotated tremor, and 8 non-PD age-matched controls). Tremor probabilities are predicted out-of-sample via the trained logistic classifier. We follow the same setup as above to obtain single daily tremor profiles per participant. Based on the assumptions in Figure 7, we condition on the presence of non-gait activity to improve the precision of tremor score estimation. We first define the intervention variable D as a binary tremor vs. non-tremor classification, where non-tremor includes both non-tremor PD and non-PD controls. Figure 9 presents both the average treatment effect estimated using the IPW estimator and the proposed dATE estimator from Section 5.2. Unlike gait energy, we observe much less overlap between the potential outcome distributions for tremor and non-tremor groups, a finding confirmed by the Welch t-test. The dynamic ATE is also significant but exhibits less structured temporal variation, likely due to tremor symptoms being less responsive to dopaminergic medication in most participants. This is further supported by the time-conditioned ATE estimates in Figure 11 (Appendix D). If we redefine D by grouping both PD cohorts together and comparing them to non-PD controls, Figure 10 shows a natural reduction in ATE differences. This aligns with the presence of low but detectable tremor probabilities in PD participants without annotated tremor. Simultaneously, the dynamic ATE effect becomes more pronounced, reflecting the periodic levodopa-induced fluctuations expected in PD tremor cases.

6 Discussion

This work introduces a novel framework for causal inference in settings involving functional data, extending traditional methods to accommodate dynamic and non-linear domains.

The primary contribution lies in studying multivariate causal effects and developing appropriate kernel methods that integrate structural assumptions about the outcome space to derive closed-form estimators of the causal effects. Specifically, the framework addresses both binary and continuous treatments with functional outcomes, demonstrating how these treatments can be modeled using Fréchet means in metric spaces such as L^2 and Fisher–Rao (Section 3.2.1 and Section 3.2.2). By leveraging operator-valued kernels, the proposed methods enable the modeling of function-valued covariates and outcomes, effectively capturing complex temporal dynamics (Section 4.1).

In comparison to existing approaches, this work generalizes prior efforts such as Ecker et al. (2024), which employ linear parametric models to estimate potential outcomes for functional data under specific assumptions, and Belloni et al. (2017), which focus on approximate local treatment effect estimators for non-Euclidean outcomes without providing finite sample inference. Unlike

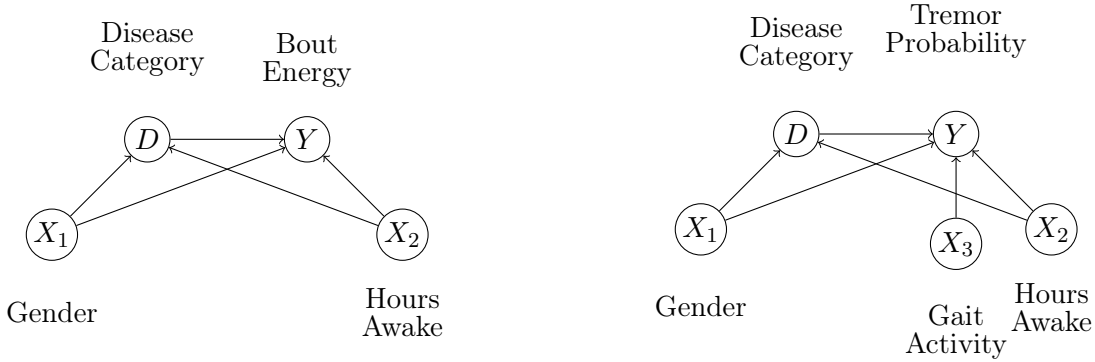


Figure 7: Causal Directed Acyclic Graphs (DAG) displaying the assumed association and its direction between estimated digital outcomes and clinical annotations. (Left) displays the minimal assumptions made for the gait bout energy, a known marker of bradykinetic gait in PD; (Right) displays the minimal assumptions made for factors affecting tremor probability estimated from a wrist-worn device.

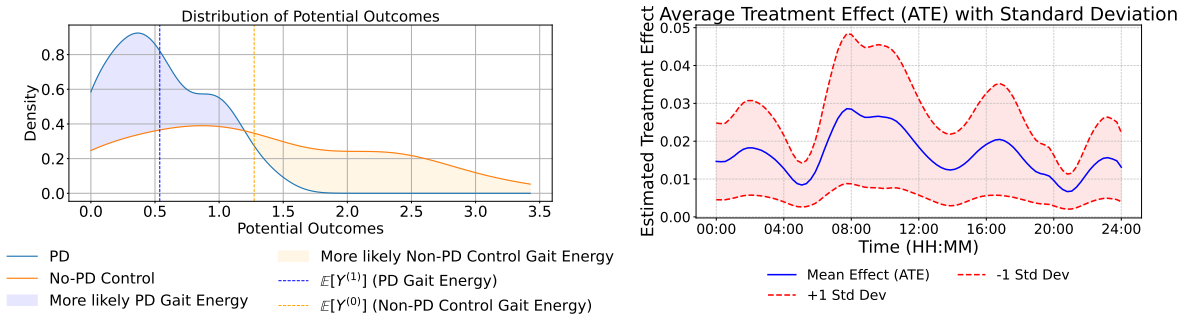


Figure 8: Effect of disease category on gait energy, estimated from average weekly digital outcomes. (Left) shows a density plot of the potential outcomes of daily outcome values for the two groups after controlling for the confounding effect of gender and hours awake using *IPW* estimator; (Right) shows the estimated dynamic average treatment effect using the proposed kernel estimator in Section 5.2. Welch t-test is performed to compare the difference in between the potential outcomes in both settings: **p-value=0.12** is obtained for the *IPW* estimator when comparing daily outcomes; **p-value<0.01** is obtained for the averaged daily potential outcomes estimated from the kernel estimator.

these works, the present framework adopts a nonparametric paradigm for estimating causal effects in infinite-dimensional functional settings, introducing joint aligning-kernelization procedures to handle path-valued random variables. Furthermore, it surpasses the methods in Singh et al. (2020), which rely on scalar outputs, by extending kernel-based causal estimators to functional outcomes. This contribution provides a more comprehensive approach to estimating causal effects on non-linear and temporally structured data.

Theorem 4 establishes the asymptotic normality of the dynamic average treatment effect (dATE) under the L^2 metric, providing theoretical guarantees for estimator reliability, while Theorem 7 formalizes the consistency of Fréchet mean estimators under the Fisher–Rao metric in functional spaces. These advancements represent significant extensions to the methods proposed by Lin et al.

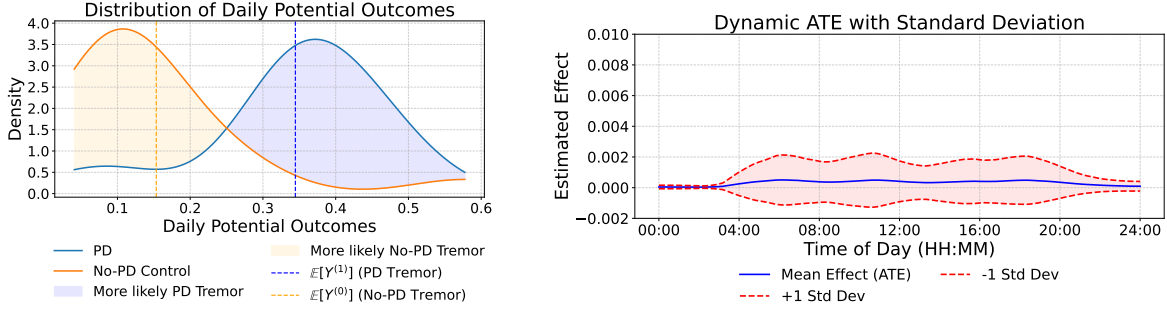


Figure 9: Effect of tremor annotation status on tremor probabilities at-home, estimated from average weekly digital outcomes. (Left) shows a density plot of the potential outcomes of daily outcome values for the two groups after controlling for the confounding effect of gender and hours awake using *IPW* estimator; (Right) shows the estimated dynamic average treatment effect using the proposed kernel estimator in Section 5.2. Welch t-test is performed to compare the difference in between the potential outcomes in both settings: **p-value**<0.01 is obtained for the *IPW* estimator when comparing daily outcomes; **p-value**<0.01 is obtained for the averaged daily potential outcomes.

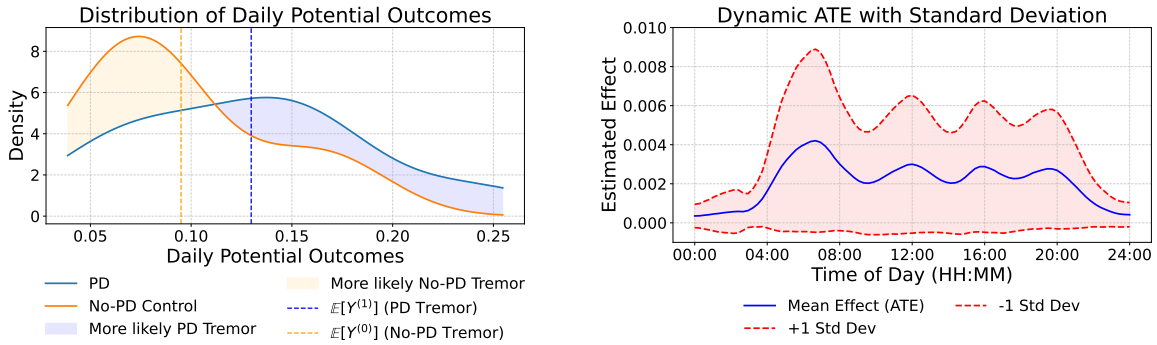


Figure 10: Effect of PD status on tremor probabilities at-home, estimated from average weekly digital outcomes. (Left) shows a density plot of the potential outcomes of daily outcome values for the two groups after controlling for the confounding effect of gender and hours awake using *IPW* estimator; (Right) shows the estimated dynamic average treatment effect using the proposed kernel estimator in Section 5.2.

(2023), by enabling causal effect estimation for complex functional outcomes and demonstrating their efficacy in high-dimensional settings. Theorem 4 complements recent work in Testa et al. (2025) with focus towards scalar treatment effect estimators.

The proposed framework is validated through extensive experiments, including synthetic setups and real-world applications to digital monitoring of PD. The experiments illustrate the ability of the framework to analyze high-dimensional functional data with temporal misalignment, evaluate more complex continuous treatment effects, and ensure appropriate estimation of the empirical estimators. In the presented PD application, we demonstrate how the dynamic ATE, φ^{dATE} , reveals different ways in which therapy affects symptoms, highlighting its previously underexplored potential (Section 5.3). In summary, this work bridges a gap in the literature by introducing a nonparametric methodology for causal inference in functional data settings, combining theoretical

rigor with practical algorithms that enable alignment. It also highlights open problems related to consistency guarantees (see Theorem 7) for causal effect estimators under more complex assumptions about the outcome and covariate spaces.

Acknowledgements

The authors wish to thank all participants in the PD@Home validation study for their enthusiasm to contribute to this study and for welcoming us into their homes. We also thank Dr. Luc J.W. Evers for his input in developing clinically relevant hypotheses in Section 5.3. Yordan P. Raykov was funded by the Michael J. Fox Foundation for Parkinson’s Research (Grants 10231 and 17369) and supported in part by the EPSRC Horizon Digital Economy Research grant Trusted Data Driven Products under Grant EP/T022493/1. Wasir R. KhudaBukhsh was supported by the Engineering and Physical Sciences Research Council (EPSRC) under Grant EP/Y027795/1.

References

- Bijan Afsari. Riemannian L^p center of mass: Existence, uniqueness, and convexity. *Proceedings of the American Mathematical Society*, 139(2):655–673, 2011.
- Andrea Aveni and Sayan Mukherjee. Uniform consistency of generalized Fréchet means. *arXiv preprint arXiv:2408.07534*, 2024.
- Alexandre Belloni, Victor Chernozhukov, Ivan Fernandez-Val, and Christian Hansen. Program evaluation and causal inference with high-dimensional data. *Econometrica*, 85(1):233–298, 2017.
- Bastiaan R. Bloem, William J. Marks, Ana Luisa Silva de Lima, Marjolein L. Kuijf, Teus Van Laar, Bastiaan P. F. Jacobs, Marcel M. Verbeek, Rick C. Helmich, Bart P. Van De Warrenburg, Laura J. W. Evers, Evelien J. Smits, Wouter Hoppenbrouwers, Marjan J. Meinders, Naud De Vries, Jacques Spies, Jorik Nonnekes, Erwin E. H. van Wegen, Karlijn Smulders, Angelo Antonini, Paolo Barone, Janet M. T. van Uem, Marc A. Hobert, Walter Maetzler, Joaquim J. Ferreira, Jao Domingos, Meir Plotnik, Lynn Rochester, Jeffrey M. Hausdorff, Anat Mirelman, Marcel O. Rikkert, and Bastiaan W. Bloem. The Personalized Parkinson Project: examining disease progression through broad biomarkers in early Parkinson’s disease. *BMC Neurology*, 19(1):160, 2019.
- Martin R Bridson and André Haefliger. *Metric spaces of non-positive curvature*, volume 319. Springer Science & Business Media, 2013.
- Siu Lun Chau, Jean-Francois Ton, Javier González, Yee Teh, and Dino Sejdinovic. BayesIMP: Uncertainty quantification for causal data fusion. *Advances in Neural Information Processing Systems*, 34:3466–3477, 2021.
- Gregory Cox. Almost sure uniqueness of a global minimum without convexity. *The Annals of Statistics*, 48(1):584–606, 2020.
- Hugh Dance, Peter Orbanz, and Arthur Gretton. Spectral representations for accurate causal uncertainty quantification with Gaussian processes. *arXiv preprint arXiv:2410.14483*, 2024.
- Rhian M. Daniel, Sara N. Cousens, Bianca L. De Stavola, Michael G. Kenward, and Jonathan A. C. Sterne. Methods for dealing with time-dependent confounding. *Statistics in Medicine*, 32(9):1584–1618, 2013.
- Kreske Ecker, Xavier de Luna, and Lina Schelin. Causal inference with a functional outcome. *Journal of the Royal Statistical Society Series C: Applied Statistics*, 73(1):221–240, 2024.
- Steven N. Evans and Adam Q. Jaffe. Limit theorems for Fréchet mean sets. *Bernoulli*, 30(1):419–447, 2024.
- Luc J.W. Evers, Yordan P. Raykov, Jesse H. Krijthe, Ana Lígia Silva de Lima, Reham Badawy, Kasper Claes, Tom M. Heskes, Max A. Little, Marjan J. Meinders, and Bastiaan R. Bloem. Real-life gait performance as a digital biomarker for motor fluctuations: the Parkinson@Home validation study. *Journal of Medical Internet Research*, 22(10):e19068, 2020.
- Luc J.W. Evers, Yordan P. Raykov, Tom M. Heskes, Jesse H. Krijthe, Bastiaan R. Bloem, and Max A. Little. Passive monitoring of Parkinson tremor in daily life: A prototypical network approach. *Sensors*, 25(2):366, 2025.
- Miguel A Hernán and James M Robins. *Causal inference*. CRC Boca Raton, FL, 2010.

- Peter J. Huber. The behavior of maximum likelihood estimates under nonstandard conditions. In *Proceedings of the Fifth Berkeley Symposium on Mathematical Statistics and Probability*, volume 1, pages 221–233. University of California Press, 1967.
- Peter J Huber and Elvezio M Ronchetti. *Robust statistics*. John Wiley & Sons, 2011.
- Kosuke Imai and David Arthur Van Dyk. Causal inference with general treatment regimes: Generalizing the propensity score. *Journal of the American Statistical Association*, 99(467):854–866, 2004.
- Hachem Kadri, Emmanuel Duflos, Philippe Preux, Stéphane Canu, Alain Rakotomamonjy, and Julien Audiffren. Operator-valued kernels for learning from functional response data. *Journal of Machine Learning Research*, 17(20):1–54, 2016.
- Edward H. Kennedy, Sivaraman Balakrishnan, and L.A. Wasserman. Semiparametric counterfactual density estimation. *Biometrika*, 110(4):875–896, 2023.
- Daisuke Kurisu, Yidong Zhou, Taisuke Otsu, and Hans-Georg Müller. Geodesic causal inference. *arXiv preprint arXiv:2406.19604*, 2024.
- Darrick Lee and Harald Oberhauser. The signature kernel. *arXiv preprint arXiv:2305.04625*, 2023.
- Zhenhua Lin, Dehan Kong, and Linbo Wang. Causal inference on distribution functions. *Journal of the Royal Statistical Society Series B: Statistical Methodology*, 85(2):378–398, 2023.
- Hengrui Luo and Justin D. Strait. Multiple closed curve modeling with uncertainty quantification for shape analysis. *SIAM/ASA Journal on Uncertainty Quantification*, 12(4):1192–1212, 2024.
- Hengrui Luo, Giovanni Nattino, and Matthew T. Pratola. Sparse additive Gaussian process regression. *Journal of Machine Learning Research*, 23(1):2652–2685, 2022.
- Charles Alden Micchelli, Massimiliano Pontil, and Peter L. Bartlett. Learning the kernel function via regularization. *Journal of Machine Learning Research*, 6(7), 2005.
- Susan A Murphy. Optimal dynamic treatment regimes. *Journal of the Royal Statistical Society Series B: Statistical Methodology*, 65(2):331–355, 2003.
- Marcus M Noack, Hengrui Luo, and Mark D Risser. A unifying perspective on non-stationary kernels for deeper Gaussian processes. *APL Machine Learning*, 2(1), 2024.
- Judea Pearl. Causal diagrams for empirical research. *Biometrika*, 82(4):669–688, 1995.
- Judea Pearl. Causal inference in statistics: An overview. *Statistics Surveys*, 3:96 – 146, 2009.
- Judea Pearl and James M. Robins. Probabilistic evaluation of sequential plans from causal models with hidden variables. In *Proceedings of the Eleventh Conference on Uncertainty in Artificial Intelligence (UAI-95)*, pages 444–453, 1995.
- J. O. Ramsay and B. W. Silverman. *Functional Data Analysis*. Springer, New York, 2005.
- James O Ramsay and Xiaochun Li. Curve registration. *Journal of the Royal Statistical Society Series B: Statistical Methodology*, 60(2):351–363, 1998.

- Yordan P. Raykov, Luc J.W. Evers, Reham Badawy, Bastiaan R. Bloem, Tom M. Heskes, Marjan J. Meinders, Kasper Claes, and Max A. Little. Probabilistic modelling of gait for robust passive monitoring in daily life. *IEEE Journal of Biomedical and Health Informatics*, 25(6):2293–2304, 2020.
- James M Robins, Andrea Rotnitzky, and Lue Ping Zhao. Estimation of regression coefficients when some regressors are not always observed. *Journal of the American statistical Association*, 89(427):846–866, 1994.
- James M Robins, Miguel Angel Hernan, and Babette Brumback. Marginal structural models and causal inference in epidemiology. *Epidemiology*, pages 550–560, 2000.
- Paul R Rosenbaum and Donald B Rubin. The central role of the propensity score in observational studies for causal effects. *Biometrika*, 70(1):41–55, 1983.
- Fredrik Sävje. Causal inference with misspecified exposure mappings: separating definitions and assumptions. *Biometrika*, 111(1):1–15, 2024.
- Christof Schötz. Strong laws of large numbers for generalizations of Fréchet mean sets. *Statistics*, 56(1):34–52, 2022.
- Rahul Singh, Liyuan Xu, and Arthur Gretton. Kernel methods for causal functions: dose, heterogeneous, and incremental response curves. *arXiv preprint arXiv:2010.04855*, 2020.
- Anuj Srivastava and Eric P Klassen. *Functional and shape data analysis*, volume 1. Springer, 2016.
- Anuj Srivastava, Wei Wu, Sebastian Kurtek, Eric Klassen, and James Stephen Marron. Registration of functional data using Fisher-Rao metric. *IEEE Transactions on Pattern Analysis and Machine Intelligence*, 33(5):954–966, 2011.
- Karl-Theodor Sturm. Probability measures on metric spaces of nonpositive curvature. In *Heat Kernels and Analysis on Manifolds, Graphs, and Metric Spaces (Paris, 2002)*, volume 338 of *Contemporary Mathematics*, pages 357–390. American Mathematical Society, Providence, RI, 2003.
- Lorenzo Testa, Tobia Boschi, Francesca Chiaromonte, Edward H. Kennedy, and Matthew Reimherr. Doubly-robust functional average treatment effect estimation. *arXiv preprint arXiv:2501.06024*, 2025.
- Sara A. van de Geer. *Empirical Processes in M-Estimation*. Cambridge University Press, 2000.
- Aad W Van der Vaart. *Asymptotic statistics*, volume 3. Cambridge University Press, 2000.

A Causal graphical models

Below, we outline some fundamental concepts frequently discussed in the causal graphical modeling literature [Pearl \(2009\)](#).

A.1 Graphs

A graph G consists of a set of directed edges E and indices $[m] = \{1, \dots, m\}$. The edges of G can be represented by a parent function $\text{pa} : [m] \rightarrow 2^{[m-1]}$, such that $l \in \text{pa}(j) \iff l \rightarrow j$ in G . If j has no incoming edges, then $\text{pa}(j) = \emptyset$. In this case, the graph G can be written as $G = (E, \text{pa})$.

A.2 Causal DAGs

A graph $G = (A, \text{pa})$ is a causal directed acyclic graph (DAG) over random variables $A := (A_i)_{i=1}^n \sim P$, if the factorization $P = \prod_i P_{i|\text{pa}(i)}$ holds, and the conditionals $(P_{j|\text{pa}(j)})_{j=1}^n$ represent actual (e.g., physical) data-generating mechanisms for observations.

Definition 10 (Back-Door Criterion, [Pearl \(1995\)](#)). Consider a causal DAG G over $(A_i)_{i=1}^n$, and let $(X, V, Y) \subseteq (A_i)_{i=1}^n$. The set V satisfies the back-door criterion with respect to (X, Y) if:

- No node in V is a descendant of X .
- V blocks every path between X and Y that contains an edge pointing into X .

Definition 11 (Front-Door Criterion, [Pearl \(1995\)](#)). Consider a causal DAG G over $(A_i)_{i=1}^n$, and let $(X, V, Y) \subseteq (A_i)_{i=1}^n$. The set V satisfies the front-door criterion with respect to (X, Y) if: (1) V intercepts all directed paths from X to Y ; (2) there is no back-door path between X and V ; (3) every back-door path between V and Y is blocked by X .

B Fisher–Rao via square-root slope functions

B.1 Square root slope functions

For function $f_i : [0, 1] \rightarrow \mathbb{R}$, we define the *square-root slope function (SRSF)* as follows:

$$q_i(t) = \text{sign}(f'_i(t)) \sqrt{|f'_i(t)|}. \quad (34)$$

Note that without loss of generality, f_i can be defined on a common closed interval $[t_1, t_m]$. We also note that given SRSF q_i , f_i can be recovered up to its starting point $f_i(0)$ via $f_i(t) = f_i(0) + \int_0^t q_i(s) |q_i(s)| ds$. Given two functions f_1, f_2 with SRSFs q_1, q_2 , the elastic pairwise registration problem means optimizing the following loss function over the group of warping functions $\Gamma = \{\gamma : [0, 1] \rightarrow [0, 1] \mid \gamma(0) = 0, \gamma(1) = 1, \gamma' > 0\}$:

$$\gamma^* = \underset{\gamma \in \Gamma}{\text{argmin}} \quad \|q_1 - (q_2 \circ \gamma) \sqrt{\gamma'}\|_{L^2}^2, \quad (35)$$

where $\|\cdot\|_{L^2}$ denotes the L^2 norm, and \circ denotes function composition. This is traditionally solved using dynamic programming or gradient-descent algorithms ([Ramsay and Li, 1998](#)). Once estimated, let $q_2^* = (q_2 \circ \gamma^*) \sqrt{\gamma^{*\prime}}$ be the optimally-warped SRSF of f_2 , and $f_2^* = f_2 \circ \gamma^*$ be the corresponding optimally-warped f_2 which is best aligned to f_1 . Estimation of γ^* can be sensitive to function noise, as taking derivatives to compute the SRSF will exacerbate the noise. As a remedy,

one can add an additional penalty term to the loss function in (35), to penalize properties of the estimated warping function (e.g., roughness).

For a collection of curves $\{f_i\}_{i=1}^n$, joint elastic registration requires one to have a template function to which all functions are jointly matched to. In the context of this work, those are selected to be estimated from the data and we adopt the *Karcher mean function* with respect to the elastic metric⁵. Karcher means are suitable for any metric space, but are particularly advantageous when closed-form sample means are not easily specified for the collection of data objects. We define the Karcher mean SRSF as:

$$\tilde{\mu}_i = \operatorname{argmin}_{q \in \mathbb{L}^2([0,1])} \sum_{i=1}^n \|q - (q_i \circ \gamma_i^*)\|_{L^2}^2 \quad (36)$$

where γ_i^* solves the pairwise registration optimization in (35). A two-step iterative algorithm is required here, as one iterates between averaging functions to form an estimate of the mean SRSF, and then performing separate pairwise alignments to align functions to this current mean SRSF estimate.

B.2 Constructing operator kernel using SRSF embedding

Proof of Theorem 9

Proof. Although one can formally define a Riemannian metric on \mathcal{F} (where \mathcal{F} is a suitable set of curves), a key result from [Srivastava and Klassen \(2016\)](#) shows that the geodesic distance under the Fisher–Rao metric between any two curves $f, g \in \mathcal{F}$ can be computed directly via their SRSFs. Concretely, we claim:

$$d_{\text{FR}}(f, g) = \|q_f - q_g\|_{L^2}.$$

To see this, construct a path $\{f_\tau\}_{\tau \in [0,1]} \subset \mathcal{F}$ corresponding to a straight line in SRSF space:

1. Let $q_f(t), q_g(t)$ be the SRSFs of f and g . A straight line in L^2 between q_f and q_g is

$$q_\tau(t) = (1 - \tau) q_f(t) + \tau q_g(t).$$

2. Define

$$f_\tau(t) = \int_0^t q_\tau(s)^2 ds.$$

Then $f_\tau(0) = 0$ and $\dot{f}_\tau(s) = q_\tau(s)^2$, so $f_\tau \in \mathcal{F}$ for each τ .

3. The Fisher–Rao length of $\tau \mapsto f_\tau$ can be shown to equal

$$\int_0^1 \left\| \frac{d}{d\tau} f_\tau \right\|_{\text{FR}} d\tau = \|q_f - q_g\|_{L^2},$$

matching the length of a straight line in L^2 .

4. One shows no other path in \mathcal{F} yields a smaller Fisher–Rao length. Thus $\|q_f - q_g\|_{L^2}$ is indeed the geodesic distance between f and g .

⁵The Karcher mean is a specific case of the Fréchet 2-mean applied in the context of Riemannian manifolds

Hence,

$$d_{\text{FR}}(f, g) = \|q_f - q_g\|_{L^2}, \quad \forall f, g \in \mathcal{F}.$$

Next we demonstrate the isometric embedding. Define

$$\Phi : \mathcal{F} \rightarrow L^2([0, 1]), \quad \Phi(f) = q_f.$$

By the above claim,

$$d_{\text{FR}}(f, g) = \|\Phi(f) - \Phi(g)\|_{L^2}.$$

Hence Φ is an *isometric embedding* of \mathcal{F} , endowed with the Fisher–Rao distance, into the Hilbert space $L^2([0, 1])$. It is injective provided we fix $f(0) = 0$ so that no two distinct curves have the same SRVF. Finally we utilize that Gaussian (RBF) Kernel is positive definite. Recall the well-known fact: if \mathcal{H} is a Hilbert space (e.g. $L^2([0, 1])$), then

$$\psi(h, h') = \exp(-\alpha \|h - h'\|^2), \quad \alpha > 0,$$

is a positive-definite kernel on \mathcal{H} . Since $\Phi : \mathcal{F} \rightarrow L^2([0, 1])$ is an isometry, define

$$k_{\text{FR}}(f, g) = \exp(-\alpha d_{\text{FR}}(f, g)^2) = \exp(-\alpha \|\Phi(f) - \Phi(g)\|_{L^2}^2).$$

For any finite set $\{f_1, \dots, f_n\} \subset \mathcal{F}$ and real coefficients $\{c_1, \dots, c_n\}$, we have

$$\sum_{i,j=1}^n c_i c_j k_{\text{FR}}(f_i, f_j) = \sum_{i,j=1}^n c_i c_j \exp(-\alpha \|\Phi(f_i) - \Phi(f_j)\|_{L^2}^2).$$

Because $\{\Phi(f_i)\} \subset L^2([0, 1])$, the standard RBF kernel in L^2 is positive-definite, so the above sum is nonnegative. Therefore, $k_{\text{FR}}(\cdot, \cdot)$ is positive definite on \mathcal{F} . Thus

$$k_{\text{FR}}(f, g) = \exp(-\alpha d_{\text{FR}}(f, g)^2)$$

is a valid positive-definite kernel on \mathcal{F} , completing the proof. \square

C Asymptotic normality of dynamic effects

C.1 Asymptotic normality of residuals in L_2

In this section, we establish the asymptotic normality of the residuals of our pointwise and norm-based estimators of the treatment effect. We first directly prove Theorem 4 for the simpler finite T case, we extend the argument as $T \rightarrow \infty$ following a functional Central Limit Theorems (fCLT) argument and point to the additional assumptions that have to be made.

Proof of Theorem 4 for finite T

Proof. Each entry $\hat{\Delta}(t)$ is an average (or difference of two averages) of i.i.d. observations, so the multivariate Central Limit Theorem ensures

$$\sqrt{n} (\hat{\Delta} - \Delta) \xrightarrow{d} \mathcal{N}(\mathbf{0}, \mathbf{K}).$$

When $\|\Delta\| \neq 0$, the map $g(x) = \|x\|_2$ is differentiable around Δ , and the usual delta method yields the normal limit with variance $\Delta^\top \mathbf{K} \Delta / \|\Delta\|_2^2$.

If $\Delta = 0$, then g is not differentiable at 0, but by the continuous mapping theorem we immediately get $\sqrt{n} \|\hat{\Delta}\|_2 \xrightarrow{d} \|\mathcal{Z}\|$ where $\|\mathcal{Z}\|$ is the Euclidean norm of a mean-zero Gaussian vector with covariance \mathbf{K} . Its square $\|\mathcal{Z}\|_2^2$ follows a generalized χ^2 -distribution (the distribution of $\sum_{j=1}^T \lambda_j \nu_j^2$ for $\nu_j \sim \mathcal{N}(0, 1)$, λ_j the eigenvalues of \mathbf{K}). \square

Infinite-dimensional extension ($T \rightarrow \infty$). Consider $\mathcal{F} = L^2([0, 1])$ with $\phi(f, g) = \langle f - g, f - g \rangle$, each observation \mathbf{Y}_i is associated with a treatment variable X_i and covariates \mathbf{V}_i . In this setting, the Fréchet mean corresponds to the pointwise, cross-sectional mean of functions, which is unique due to the strict convexity of the squared L_2 norm.

Proof. For the infinite dimensional setting, a similar argument for asymptotic normality of the estimator residuals can be made using some recent results from [Kennedy et al. \(2023\)](#) demonstrating that under standard *identifiability* assumptions outlined above, the defined functional potential outcomes $\mathbf{Y}^{(1)}$ and $\mathbf{Y}^{(0)}$ belong to the Donsker class (a formal proof is provided as a special case of ([Kennedy et al., 2023](#), Theorem 3)). If, instead of a fixed dimension T , the potential outcomes $\mathbf{Y}^{(1)}$ and $\mathbf{Y}^{(0)}$ are functions in a suitable infinite-dimensional space (e.g. $L_2([0, 1])$), one can invoke a *functional* CLT. Under conditions ensuring that the empirical processes $\hat{F}(\mathbf{Y}^{(x)})$ converge in distribution in some function space (often requiring $\mathbf{Y}^{(x)}$ to lie in a Donsker class, see [Van der Vaart \(2000\)](#); [Kennedy et al. \(2023\)](#)), one obtains

$$\sqrt{n}[\hat{F}(\mathbf{Y}^{(1)}) - F(\mathbf{Y}^{(1)})] \xrightarrow{d} \mathcal{GP}^{(1)}, \quad \sqrt{n}[\hat{F}(\mathbf{Y}^{(0)}) - F(\mathbf{Y}^{(0)})] \xrightarrow{d} \mathcal{GP}^{(0)},$$

where $\mathcal{GP}^{(1)}, \mathcal{GP}^{(0)}$ are mean-zero Gaussian *processes*. Hence their difference is also asymptotically Gaussian in the relevant function space:

$$\sqrt{n}(\hat{\Delta}(\cdot) - \Delta(\cdot)) = \sqrt{n}[\hat{F}(\mathbf{Y}^{(1)}) - F(\mathbf{Y}^{(1)})] - \sqrt{n}[\hat{F}(\mathbf{Y}^{(0)}) - F(\mathbf{Y}^{(0)})] \xrightarrow{d} \mathcal{GP}^{(1)} - \mathcal{GP}^{(0)}.$$

Applying the *functional* delta method to the map $\Delta(\cdot) \mapsto \|\Delta(\cdot)\|_{L^2}$ requires Fréchet differentiability at non-zero Δ . The derivative of $\|\cdot\|_{L^2}$ at Δ is

$$h'_\Delta(g) = \frac{\langle g, \Delta \rangle_{L^2}}{\|\Delta\|_{L^2}} \quad \text{for } \|\Delta\| \neq 0.$$

From this, one obtains precisely the same asymptotic normality result for $\sqrt{n}(\|\hat{\Delta}\|_{L^2} - \|\Delta\|_{L^2})$, but with $\mathcal{GP}^{(x)}$ now interpreted as infinite-dimensional Gaussian processes (and their inner products with Δ giving the limiting variance). For the zero-function case $\|\Delta\|_{L^2} = 0$, one again obtains convergence in distribution to the norm of a mean-zero Gaussian process, i.e. $\|\mathcal{Z}\|_{L^2}$ for \mathcal{Z} in a suitable function space; see ([Testa et al., 2025](#), Theorem 3.9) for a more detailed study of the asymptotic normality of the residuals of $\hat{\Delta}$ in the functional setting. For the infinite-dimensional scenario, the primary additional requirement is that the *class* of (potential) outcome functions $\mathbf{Y}^{(1)}(\cdot)$ and $\mathbf{Y}^{(0)}(\cdot)$ be Donsker (ensuring a functional CLT), and that the map $\Delta(\cdot) \mapsto \|\Delta(\cdot)\|_{L^2}$ be sufficiently regular (Fréchet differentiable away from zero). Under these assumptions, all the conclusions of Theorem 4 extend naturally to $T \rightarrow \infty$. \square

C.2 Consistency of Fréchet mean estimators under Fisher–Rao

Proof. The idea of our proof is as follows, we restrict the vector domain \mathcal{T} so small that the $\phi(\mathbf{Y}, \mathbf{g})$ is injective and nearly linear in each of these T -coordinates in \mathbf{Y} when domain \mathcal{T} is assumed; then we verify the (A1)-(A5) in [Huber \(1967\)](#) to elicit the \bar{f}_n as a consistent solution to the finite dimensional minimization problem; then we need to verify assumptions of Lemma 1 in [Cox \(2020\)](#) to ensure that this solution is unique.

Step 1: injectivity. The function $f(a_1, \dots, a_T) = \sum_{i=1}^T w_i \sqrt{a_i}$ is injective if each unique input (a_1, \dots, a_T) produces a distinct output. Suppose $f(a_1, \dots, a_T) = f(b_1, \dots, b_T)$, which implies

$$\sum_{i=1}^T w_i (\sqrt{a_i} - \sqrt{b_i}) = 0.$$

To ensure injectivity under assumption, we impose the constraint $a_1 \leq a_2 \leq \dots \leq a_T$, which prevents any swapping of values between indices. To prove injectivity under this constraint, assume $f(a_1, \dots, a_T) = f(b_1, \dots, b_T)$. Starting with the largest term $w_T \sqrt{a_T}$, it corresponds uniquely to the largest weight w_T , so $a_T = b_T$. Subtracting $w_T \sqrt{a_T}$ from both sides reduces the problem to

$$\sum_{i=1}^{T-1} w_i \sqrt{a_i} = \sum_{i=1}^{T-1} w_i \sqrt{b_i}.$$

By induction, $a_i = b_i$ for all i . Thus, $f(a_1, \dots, a_T)$ is injective on the domain

$$\mathcal{D} = \{(a_1, \dots, a_T) \in [0, \infty)^T \mid a_1 \leq a_2 \leq \dots \leq a_T\}.$$

Step 2: almost sure uniqueness. Since the ϕ is not necessarily convex in \mathbb{R}^T , the uniqueness result for M -estimators cannot apply directly. We prove that the resulting *argmin* is unique by verifying the following three assumptions in the Lemma 1 of [Cox \(2020\)](#).

- (Absolute Continuity) The function $\phi(\mathbf{Y}_i, \mathbf{g})$ is absolute continuous in $\mathcal{T} \subset \mathbb{R}^T$ from its definition (18), and it is supported on the whole $\mathcal{T} \subset \mathbb{R}^T$.
- (Manifold) The minimization is solved over $\mathcal{T} = \mathbb{R}^T$, which is a disjoint union of countably many second-countable Hausdorff manifolds consisting of only one element \mathcal{T} .
- (Continuous Differentiability) There are three assumptions (a) - (c) to be verified: (a) $\phi(\mathbf{Y}_i, \mathbf{g})$ is a continuous function of $\mathbf{g} \in \mathcal{T}$ and $\mathbf{Y}_i \in \mathcal{T} \subset \mathbb{R}^T$ from definition (18) and the continuity of arccos and square root. (b) For every $\mathbf{Y}_i \in \mathcal{T}$ and $\mathbf{g} \in \mathcal{T}$, $\phi(\mathbf{Y}_i, \mathbf{g})$ is differentiable with respect to \mathbf{Y} 's, and the derivative is continuous with respect to \mathbf{g} and \mathbf{Y} . The derivative of arccos over \mathcal{T} is continuous since it does not attain the value $1/T$, which we exclude from our \mathcal{T} 's. (c) For every $\mathbf{Y}_i \in \mathbb{R}^T$, $\mathbf{g} \in \mathcal{T}$, and for $\Delta \in A(\mathbf{g})$ as the T -dimensional tangent cone of \mathbf{g} to \mathcal{T} , $\phi(\mathbf{Y}_i, \mathbf{g})$ is differentiable with respect to \mathbf{g} in the direction and the derivative is continuous with respect to \mathbf{Y} and \mathbf{g} . This follows from the (b) and the fact that the \mathcal{T} has a flat geometry (Also see [Cox \(2020\)](#)'s Remark 1).

(Generic, the assumption a) Let $\xi(\mathbf{g}_1, \mathbf{g}_2, \mathbf{Y}) = \phi(\mathbf{g}_1, \mathbf{Y}) - \phi(\mathbf{g}_2, \mathbf{Y})$, then on

$$\Xi = \{(\mathbf{g}_1, \mathbf{g}_2, \mathbf{Y}) : \mathbf{Y} \in \mathcal{T}, \mathbf{g}_1, \mathbf{g}_2 \in \mathcal{T}, \mathbf{g}_1 \neq \mathbf{g}_2\},$$

$\xi(\mathbf{g}_1, \mathbf{g}_2, \mathbf{Y}) \neq 0$ due to the restriction of the domain of $[0, 1/T - \delta/T]^T$. If every $Y_i(j), g_j$ in definition (18) is strictly less than $1/T$, then $\sum_{j=1}^T \sqrt{Y_i(j)g_j} < 1$ and we know that arccos does not have zero point within $(-1, 1)$.

Step 3: Consistency. Suppose we observe i.i.d. samples $\mathbf{Y}_1, \dots, \mathbf{Y}_n \in \mathbb{R}^T$ of size n drawn from a common distribution P_x supported on $\mathcal{T} \subset \mathbb{R}^T$. Denote by $\mathcal{B}(\mathbb{R}^T)$ the Borel σ -algebra on \mathbb{R}^T , and assume that P_x has finite second moments; that is,

$$\int_{\mathbb{R}^T} \|\mathbf{y}\|^2 P_x(d\mathbf{y}) < \infty.$$

For instance, a “true” function \bar{f} evaluated at T time points, $(\bar{f}(1), \dots, \bar{f}(T))$, plus i.i.d. Gaussian noise $(\bar{f}(1) + \epsilon_1, \dots, \bar{f}(T) + \epsilon_T)$, where each $\epsilon_i \sim N(0, \sigma^2)$, will satisfy this assumption.

Let \bar{f}_n be the Fréchet mean estimator of \bar{f} defined by

$$\frac{1}{n} \sum_{i=1}^n \phi(\mathbf{Y}_i, \bar{f}_n) - \inf_{g \in \mathbb{R}^T} \frac{1}{n} \sum_{i=1}^n \phi(\mathbf{Y}_i, g) \xrightarrow{n \rightarrow \infty} 0,$$

where ϕ is our chosen distance (e.g., squared Euclidean or a Fisher–Rao metric). Following [Huber \(1967\)](#), one shows that $\bar{f}_n \rightarrow \bar{f}$ in probability (and a.s.) under P_x by verifying Huber’s conditions (A1)–(A5):

(A1) For each fixed \mathbf{g} , $\phi(\mathbf{Y}, \mathbf{g})$ is \mathcal{A} -measurable, which follows from its definition (18), and its Doob separability comes from the assumption on \mathcal{T} such that every $Y_i(j), g_j$ in definition (18) is strictly less than $1/T$, then $\sum_{j=1}^T \sqrt{Y_i(j)g_j} < 1$ and injective on \mathcal{D} , and arccos is injective on $(0, 1)$.

(A2) The function $\phi(\mathbf{Y}, \mathbf{g})$ is differentiable, hence P_x -a.s. lower semicontinuous.

(A3) There is a measurable function $a(\mathbf{Y}) = a_\delta(\mathbf{Y}) = \inf_{\mathbf{g} \in \mathcal{T}} \phi(\mathbf{Y}, \mathbf{g})$ (or sup) since the domain \mathcal{T} is a compact domain and $\sum_{j=1}^T \sqrt{Y_i(j)g_j} \leq \sum_{j=1}^T (1/T - \delta/T) \leq 1 - \delta < 1$.

$$\mathbb{E}_P (\phi(\mathbf{Y}, \mathbf{g}) - a(\mathbf{Y}))^- < \infty$$

$$\mathbb{E}_P (\phi(\mathbf{Y}, \mathbf{g}) - a(\mathbf{Y}))^+ < \infty$$

and therefore $\gamma(\mathbf{g}) = \mathbb{E}(\phi(\mathbf{Y}, \mathbf{g}) - a(\mathbf{Y}))$ is well-defined for all $\mathbf{g} \in \mathcal{T}$.

(A4) There is a \mathbf{g}_0 such that $\gamma(\mathbf{g}) \geq \gamma(\mathbf{g}_0)$ for all $\mathbf{g} \in \mathcal{T}$, follows from argument in (A3) and taking the derivative inside \mathbb{E}_{P_x} . Then within the same domain \mathcal{T} , the $\phi(\mathbf{Y}, \mathbf{g})$ is monotonic along each of T coordinate, the \mathbf{g}_0 exists, and is essentially unique with respect to $P_x^{(n)}$ from our argument in step 2.

(A5) Since the domain \mathcal{T} is compact, it suffices to verify that $\inf_{\mathbf{g} \in \mathcal{T}} \frac{\phi(\mathbf{Y}, \mathbf{g}) - a(\mathbf{Y})}{b(\mathbf{g})} \geq 0$, and take the $h(\mathbf{Y}) = 0$; any positive $b(\mathbf{g})$ will suffice. \square

This sufficiency result is interesting in application, it means that the uniqueness of empirical Fréchet mean is ensured in a narrower and narrower cube, as the number of sample points T over the grid increases. In other words, if we have more and more sample points, there could be identifiability issue, warning us of the “extra-flexibility” brought by functional data. However, since our condition is only sufficient, there could be a wider domain (e.g., removing the monotonicity induced by \mathcal{D}) where the uniqueness is ensured.

D Digital outcomes for Parkinson’s disease

D.1 Features for symptom detection

Within stationary segments, 28 different features are extracted from each axis of the pre-processed accelerometer data, based on non-overlapping 5 second windows: the standard deviation; the power in different frequency bands (0.3-2Hz, 4-8Hz, 8-12Hz, 0.2-14Hz); the frequency and height of the dominant peak in the PSD within different frequency bands (0.3-2Hz, 4-8Hz, 8-12Hz, 0.2-14Hz); the sample entropy, and the spectral entropy; 13 mel cepstral coefficients. We then perform z-score normalization of the feature vectors, using the data from the unscripted activities of all 24 PD patients (both with and without annotated tremor episodes) and all 24 non-PD controls. These features are then used to train a logistic classifier (i.e., applying l_1 -regularization) to predict the annotated gait and tremor episodes in the home visits segment of the Parkinson@Home cohort. The performance measures for both classifiers are computed using leave-one-subject-out cross validation and are reported in Table 5.

Table 4: Demographic and clinical characteristics of PD patients and non-PD controls included in the analyses. IQR: inter-quartile range. MDS-UPDRS: Movement Disorder Society-Sponsored Revision of the Unified Parkinson’s Disease Rating Scale. Part 1: non-motor experiences of daily living. Part 2: motor experiences of daily living. Part 3: motor examination. Part 4: motor complications. *: 1 missing value.

PD patients with annotated tremor ($n = 8$)	
61.0 (58.3 - 69.0)	
Gender (men), n (%)	
Time since diagnosis of PD (years), median (IQR)	
Hoehn and Yahr stage in off state, n (%)	
Stage 1	
Stage 2	
Stage 3	
Stage 4	
MDS-UPDRS, median (IQR)	
Part 1	(scale range: 0 to 52)
Part 2	(scale range: 0 to 52)
Part 3 (off state)	(scale range: 0 to 132)
Part 3 (on state)	(scale range: 0 to 132)
Part 4	(scale range: 0 to 24)
Tremor sub-score of MDS-UPDRS part III, median (IQR)	
Off state	(scale range: 0 to 40)
On state	(scale range: 0 to 40)
Rest tremor severity (arm of most affected side), n (%)	
0: normal (off on)	
1: slight (off on)	
2: mild (off on)	
3: moderate (off on)	
4: severe (off on)	

D.2 Annotation protocol

If the patient performed significant upper limb activities for more than 3 seconds, the assistant only annotated whether tremor was present or not. Otherwise, both the presence and severity of the tremor were annotated, similar to the MDS-UPDRS part III tremor items. However, because of the low prevalence of moderate and severe tremor in this dataset, we aimed to model only the presence of tremor.

D.3 Conditional Treatment Effects

To provide context on the digital monitoring application discussed in Section 5.3, we estimate the conditional ATE using the standard IPW estimator [Imai and Van Dyk \(2004\)](#), explicitly conditioning on the time covariate. Figure 11 presents the mean and standard deviation of the potential outcomes for both the treated and non-treated groups. We observe that the more complex causal estimators yield a similar dynamic ATE for the effect of levodopa therapy on gait energy. However, while the IPW conditional ATE estimator obscures the significance of the therapy’s effect on tremor episodes,

Event detection	AUROC	Sensitivity	Specificity
Tremor detection	0.89 (0.07)	0.74 (0.16)	0.95 (0.07)
Gait detection	0.95 (0.03)	0.73 (0.17)	0.95 (0.04)

Table 5: Performance metrics for tremor and gait detection algorithms trained and evaluated from the Parkinson@Home annotated visits. We use leave-one-subject-out cross-validation; mean measures across folds are reported with standard deviation in the brackets.

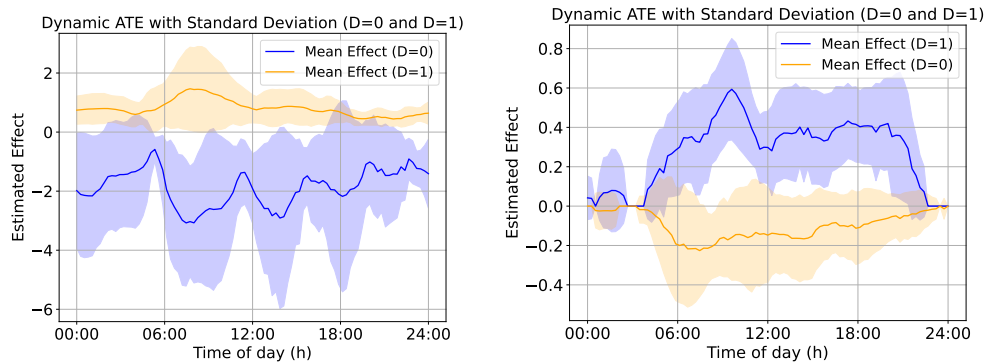


Figure 11: Average effect of disease category on digital outcomes (left) gait, (right) tremor. IPW estimator is used to condition explicitly on time and display the φ^{cATE} estimator on the time grid.

the purpose-designed functional causal kernel ATE estimator better highlights this effect.